RESEARCH ARTICLE

Thermodynamics and airstreams of a south foehn event in different Alpine valleys

Lukas Jansing | **Michael Sprenger**

Institute for Atmospheric and Climate Science, ETH, Zurich, Switzerland

Correspondence
L. Jansing, IAC, ETH Zürich, Universitätstrasse 16, Zürich 8092, Switzerland.
Email: lukas.jansing@env.ethz.ch

Abstract

Foehn flows are associated with a characteristic warming of the respective air in lee-side valleys. Recent studies about the physical mechanisms question the traditional thermodynamic foehn theory, pointing out the potential role of adiabatic descent and other diabatic processes, besides upstream latent heating in clouds, for the warming. This study applies a kilometre-scale simulation together with online trajectories and a Lagrangian heat budget to investigate the foehn air warming for an intense, long-lasting Alpine south foehn period in November 2016. Thereby, the focus lies on the attribution of the warming to adiabatic descent and the different diabatic processes in six foehn valleys, as well as the linkage of the warming processes to different airstreams. Overall, adiabatic warming emerges as the most important process for 57% of all air parcels arriving in the foehn valleys. However, upstream latent heating in clouds is the dominant mechanism for a considerable amount of air parcels (35%). The heat budget analysis reveals a clear transition along the Alps from west to east, whereat diabatic warming constitutes the driving mechanism for western valleys during the central phase of the event, and adiabatic warming dominates the foehn air warming in eastern valleys. The foehn trajectories can be separated into different air-stream categories according to their diabatic temperature change. Air parcels experiencing strong diabatic heating are transported in an easterly barrier jet in the Po Valley before crossing the Alpine crest. Air parcels experiencing diabatic cooling, in contrast, are advected quasi-horizontally from the south towards the Alpine crest prior to their descent. The relative strength of the different airstreams therefore determines the dominating warming process. These findings strongly point to the combined importance of adiabatic *and* diabatic warming mechanisms, which co-occur with varying relative contributions, depending on the valley and time period of the event.

KEYWORDS

airstreams, Alpine south foehn, foehn air warming, Lagrangian heat budget, trajectories

Lukas Jansing and Michael Sprenger contributed equally to this work.

1 | INTRODUCTION

The term foehn represents a generic expression for downslope winds occurring whenever the atmospheric flow needs to overcome orographic obstacles. These winds exhibit archetypal characteristics, as they are warm, dry, and often gusty in nature. Their frequent occurrence is recognised in various regions of the world, among them being the Chinook in the western United States (Glennf, 1961), the Puelche in Chile (Beusch *et al.*, 2018; Montecinos *et al.*, 2017), and the Inami-kaze in Japan (Koyanagi and Kusaka, 2020). Their socio-economic impact has been stated in terms of increased risk for wildfire ignition and spread (Sharples *et al.*, 2010) or infrastructural damage and a risk for aviation (Richner and Hächler, 2013). Furthermore, they affect agricultural production in foehn regions. Whereas foehn winds are found to promote white head occurrence on Japanese rice plantations (Asano and Kusaka, 2021), anecdotal evidence indicates that they are beneficial for wine production in Alpine foehn valleys (Walker and Ruffner, 1998). Recently, foehn flows have also been attributed a key role for surface melt on the Larsen C Ice Shelf in Antarctica (Elvidge *et al.*, 2020) and in northeast Greenland (Mattingly *et al.*, 2020).

The Alpine foehn has been in the focus of research for over two centuries. Whereas the pronounced warming in valleys north of the Alps during south foehn onset is a well-known fact (Richner and Hächler, 2013; Sprenger *et al.*, 2016; Steinacker, 2006), a long-lasting debate about the physical reasoning persists. Hann (1866) was among the first emphasising the importance of upstream latent heating for the warmth of the foehn air. Later, he put his considerations into perspective by mentioning the occurrence of foehn events without upstream precipitation and the role of adiabatic warming during the descent (Hann, 1885). Nevertheless, his original conceptions became a dominating paradigm (Seibert, 2005). More recently, multiple studies have re-emphasised the key role of lee-side adiabatic compression of air originating from elevated upstream levels, being decoupled from the blocked air mass underneath (e.g., Seibert, 1990). Elvidge *et al.* (2015) and Miltenberger *et al.* (2016) referred to this process as the "isentropic drawdown" mechanism. These more recent studies indicate that several processes can, in fact, contribute to the foehn air warming with varying importance. Likewise, the Mesoscale Alpine Programme (Bougeault *et al.*, 2001), which took place in the late 1990s, revealed a substantial case-to-case variability. Some intensive observation periods (IOPs) were associated with widespread and intense upstream precipitation (e.g., IOP 2; Richner *et al.*, 2006; Rotunno and Houze, 2007). In contrast, other cases in fact almost completely lacked precipitation (e.g., IOP 13;

Richner *et al.*, 2006). For some IOPs, in turn, the upstream air mass over the Po Valley was decoupled from the flow aloft and formed an easterly barrier jet (Bousquet and Smull, 2003). The pronounced case-to-case differences, as observed during the Mesoscale Alpine Programme, indicate that isentropic drawdown or latent heating can both govern the foehn air warming for south foehn events.

Besides these differing explanations for the foehn air warming, the phenomenon can also be considered from two contrasting perspectives: In an Eulerian framework, the foehn air warming depends on the temperature difference of the foehn air and the precedent valley air mass. The magnitude of the warming is thus affected by the strength of the cold pool, which is oftentimes present in the valleys prior to foehn breakthrough (e.g., Drobinski *et al.*, 2007). Glennf (1961) already mentioned this air mass replacement as one of the possible processes for the warming of the Chinook. Foehn–cold-pool interaction and the erosion of cold pools still constitutes a field of active research on the Alpine foehn (e.g., Haid *et al.*, 2020; Umek *et al.*, 2021). Refocusing on the warming, newer studies usually invoked the Lagrangian perspective following the motion of air parcels. Increasing resolution of numerical weather prediction (NWP) models allows for the calculation of air parcel trajectories over complex mountainous terrain, including the descent of air into specific foehn valleys. Consequently, they have been applied to study the origin of foehn air parcels arriving in Innsbruck (Seibert *et al.*, 2000), to elucidate the role of foehn effects on the formation of an extreme temperature event near Tokyo (Takane and Kusaka, 2011), or to investigate the effect of the upstream flow regime on the downstream foehn development along the Antarctic Peninsula (Elvidge *et al.*, 2014). Würsch and Sprenger (2015) performed a Lagrangian analysis for an extensive period covering 3 years of foehn events in Altdorf (Switzerland) and Ellbögen (Austria). They revealed pronounced regional differences. Altdorf trajectories experience a larger moisture loss and are more often related to precipitation than the Ellbögen ones. Hence, the analysis corroborates the distinction of a "Swiss foehn" and an "Austrian foehn" as proposed by Steinacker (2006), whereas the former more closely follows the thermodynamic foehn theory. Similarly, Kusaka *et al.* (2021) investigated a multitude of south foehn events in Japan. According to their backward trajectory analysis, adiabatic compression (isentropic drawdown) governs the foehn air warming for most cases. Moreover, the trajectories show that, even during events with precipitation, not all air parcels are subject to strong ascent. This finding illustrates the complex nature of foehn flows and highlights a finding that cannot be derived by merely considering Eulerian fields.

The combined usage of air parcel trajectories with heat budget methodologies also allows for a more comprehensive assessment of the foehn air warming. Miltenberger *et al.* (2016) quantified the contribution of microphysical processes to the potential temperature change for an Alpine south foehn case. They however left out the effects of turbulent mixing and radiation and focused on one major foehn valley (Rhine Valley). Interestingly, they found a relation between the magnitude and sign of the potential temperature change and the cross-Alpine net vertical displacement of air parcels, referred to as the "scrambling" of air parcels, a concept originally introduced by Smith *et al.* (2003). This finding still needs to be confirmed by other case studies. Furthermore, it is unclear whether different warming processes can be attributed to distinct airstreams on the southern side of the Alps, too. Saigger and Gohm (2022) identified two airstreams with contrasting diabatic temperature evolution contributing to a west foehn event in the Inn Valley. Their results highlight the potential linkage of different warming mechanisms to distinct airstreams, while they refrained from an explicit quantification of the contribution of turbulence and radiation towards the heating. Takane *et al.* (2015) and Elvidge and Renfrew (2016) applied heat budget analyses including the diabatic effects of sensible heating and turbulent mixing and radiation, respectively. According to Elvidge and Renfrew (2016), each of the potential mechanisms, namely adiabatic compression, upstream latent heating in clouds, and turbulent downward mixing of potentially warmer air, can be of key importance for the warming, depending on the case study. However, it remains unclear whether their findings can be transferred from the Antarctic Peninsula to the Alpine region. Therefore, the main research questions tackled in this article narrow down to the following:

1. Which processes are responsible for the foehn air warming along trajectories arriving in different Alpine foehn valleys?
2. To what extent do differential thermodynamic properties of trajectories relate to origin and pathway of windward airstreams?
3. What is the temporal evolution of the airstreams during the foehn event in the six Alpine valleys?

These research questions are addressed by focusing on a long-lasting foehn event from November 20 to 24, 2016. The main novelty of this study is the comparison of foehn air warming processes in six Alpine valleys during the same event, using online trajectories in an NWP simulation with 1 km grid spacing. In addition, we present a Lagrangian heat budget considering both adiabatic warming and all diabatic processes (cloud microphysics, turbulence, radiation) as potential warming mechanisms for foehn air parcels.

When studying foehn flows with mesoscale models, it needs to be kept in mind that these models usually exhibit distinct biases related to surface variables, namely a cold bias and a moist bias during foehn hours. These biases have been described by the Consortium for Small-scale Modeling (COSMO) for 2.2 km horizontal grid spacing (COSMO-2) in Switzerland (Wilhelm, 2012) and for 1.1 km horizontal grid spacing (COSMO-1) in Austria (Sandner, 2020). However, according to Gerstgrasser (2017), the moist bias already halved for COSMO-1 compared with COSMO-2. Additionally, Wilhelm (2012) found a decreasing bias for higher model levels. Schmidli *et al.* (2018) compared the skill of COSMO-2 and COSMO-1 in simulating thermally driven valley wind systems and noted a considerable increase in accuracy when moving to 1 km grid spacing. Therefore, we are confident that our model set-up is applicable to study detailed aspects of a south foehn case in the Alpine region.

The remainder of the paper is structured as follows: In Section 2 we present our main methodology, including the set-up of the NWP model for the case study from November 19 to 25, the trajectory calculations, and the Lagrangian heat budget. We then present the distinct synoptic- and mescoscale flow evolution of the event (Section 3), followed by a detailed analysis of the foehn air-warming mechanisms (Section 4). Thereafter, we subdivide the trajectories into three air-stream categories based on their diabatic heating strength and analyse the temporal evolution of the airstreams as well as their characteristic cloud and precipitation patterns (Section 5). Section 6 summarises the key findings.

2 | NUMERICAL MODEL AND LAGRANGIAN DIAGNOSTICS

2.1 | The COSMO model

The COSMO limited-area model is a non-hydrostatic NWP model that integrates the thermo-hydrodynamical equations on a structured grid (Steppeler *et al.*, 2003). It has been developed for and extensively tested at the convection-permitting scale both for operational forecasting (Baldauf *et al.*, 2011) and scientific applications (e.g., Ban *et al.*, 2014). This study employs COSMO version 5.6 according to the operational COSMO-1 set-up at the Swiss national weather service MeteoSwiss. The simulation domain covers the greater Alpine region (Figure 1a) and was conducted with a horizontal grid spacing of 1.1 km, 80 vertical levels, and a time step of 10 s. Whereas cloud processes were parametrised using a single-moment bulk
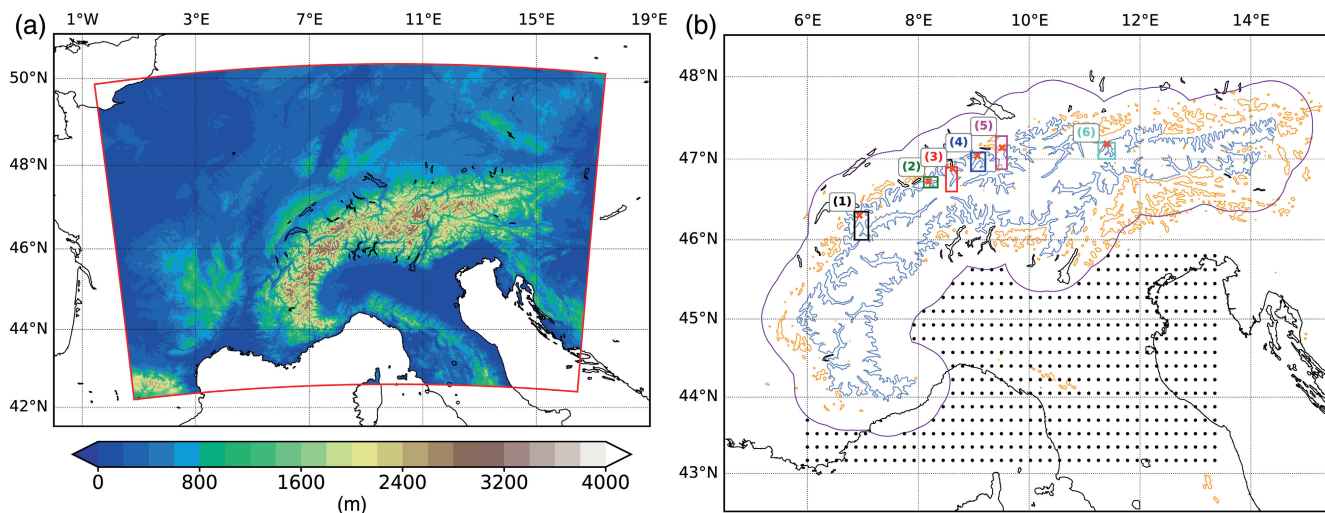
FIGURE 1 (a) COSMO-1 model domain and topography. (b) The trajectory starting points (black dots), the 50 km polygon (violet contour), the closed 1,500 m contour of the Alpine arc (blue), additional 1,500 m contours (orange), valley boxes for the different valleys—(1) Lower Valais; (2) Hasli Valley; (3) Reuss Valley; (4) Linth Valley; (5) Rhine Valley; (6) Wipp Valley—and the foehn locations (red crosses). An enlarged overview map covering the relevant part of the Alps is included in the supplement (Figure S1) [Colour figure can be viewed at wileyonlinelibrary.com]

mycrophysics scheme including five prognostic hydrometeor classes (Reinhardt and Seifert, 2006), all convection parametrisations were switched off. Additional active parametrisations include radiative transfer (Ritter and Geleyn, 1992), vertical turbulent diffusion and surface fluxes (Mellor and Yamada, 1982; Raschendorfer, 2001), and soil processes (Heise *et al.*, 2006). In the context of this study, COSMO-1 is used to perform a hindcast of a specific south foehn event. The model was initialised at 1800 UTC on November 19, 2016, and ran for the subsequent 6 days (144 hr). Operational COSMO-1 analyses from MeteoSwiss at the same spatial resolution as the hindcast served as initial and boundary conditions for the integration, thereby preventing the necessity of additional spin-up time. Three-dimensional model output was written to disk in 10-min intervals.

2.2 | Online trajectory calculation and selection

Miltenberger *et al.* (2013) incorporated an online trajectory module into the COSMO model. This allows for the calculation of Lagrangian air parcel trajectories online during model integration, thereby making use of the wind fields at each native model time step. The benefits of online trajectories are particularly large in regions where topography modulates the atmospheric flow, and trajectories calculated with input fields at lower temporal resolution can deviate drastically (Miltenberger *et al.*, 2013). The sensitivity experiments of Saigger (2021) indicate that

the solution of the trajectory integration does not yet converge with an input interval of 5 min, which points out the gain of online trajectories in the context of foehn events. Inherent to the forward integration of the COSMO model, the module only allows for calculation of forward trajectories. Therefore, it is necessary to sample the full volume of air potentially contributing to the foehn flow within different valleys. To this end, starting points have been defined in a three-dimensional latitude–longitude box on the Alpine south side (6–13.35°E, 43.175–45.8°N) with a horizontal spacing of 0.175° and a vertical spacing of 250 m reaching up to 5 km (Figure 1b). The lower limit of the box is set to 20 m above the surface. The goal of this study is to sample the full history of air parcels crossing the Alpine arc. Therefore, in order to prevent the initialisation of trajectories over mountainous terrain, the box is cropped by a polygon with 50 km distance to the innermost closed 1,500 m contour of the Alps. This design results in 9,394 trajectories per starting time. Trajectories were released in two-hourly intervals starting from 1800 UTC on November 19, 2016, until 1200 UTC on November 25, 2016, each calculated until reaching a length of 36 hr. Besides the standard prognostic variables, all diabatic temperature tendencies were traced along the trajectories (see also Section 2.3). For the detailed heat budget and air-stream analysis, output was written at the highest possible temporal resolution (10 s).

The study focuses on six major foehn valleys (Figure 1b). To classify trajectories as foehn trajectories, a simple geographic criterion is applied: For each valley, a bounding box is defined. A trajectory is selected

TABLE 1 Table providing the information on the bounding boxes, foehn locations, and altitude thresholds for the six different valleys

Valley	Bounding box	Foehn location	Altitude (800 m AGL)
Lower Valais (1)	6.85–7.1°E, 46.0–46.35°N	Aigle (6.94°E, 46.30°N)	1,166.4 m
Hasli Valley (2)	8.1–8.35°E, 46.65–46.78°N	Meiringen (8.19°E, 46.73°N)	1,443.8 m
Reuss Valley (3)	8.5–8.7°E, 46.6–46.9°N	Altdorf (8.62°E, 46.88°N)	1,241.3 m
Linth Valley (4)	8.95–9.21°E, 46.85–47.08°N	Glarus (9.07°E, 47.04°N)	1,370.1 m
Rhine Valley (5)	9.4–9.6°E, 46.875–47.28°N	Vaduz (9.51°E, 47.14°N)	1,242.2 m
Wipp Valley (6)	11.25–11.55°E, 47.0–47.2°N	Schönberg (11.40°E, 47.19°N)	1,740.7 m

Note: The number after a valley's name refers to the corresponding boxes in Figure 1b.

if it passes through this valley box and descends below 800 m above the altitude of a predefined foehn location within each box at the time instant when its latitude is closest to the latitude of the foehn location. Thereby, the location-dependent altitude threshold ensures that only air parcels descending well into the valley atmosphere are classified as foehn trajectories (see also Table 1).

2.3 | Lagrangian heat budget

Similar to recent studies on foehn air warming (Elvidge and Renfrew, 2016; Miltenberger *et al.*, 2016; Takane *et al.*, 2015), a Lagrangian heat budget is applied to the air parcel trajectories in order to quantify the warming mechanisms. The formulation, however, differs slightly from earlier publications and is therefore briefly discussed here. The thermodynamic energy equation describes the differential change in temperature T following the motion of the flow as a sum of an adiabatic and a diabatic source term:

$$\frac{DT}{Dt} = \frac{\kappa T \omega}{p} + \frac{D\theta}{Dt} \cdot \left(\frac{p_0}{p}\right)^{-\kappa}. \quad (1)$$

Thus, Equation (1), with $\kappa = R/c_p = 0.286$, $\omega = Dp/Dt$, reference pressure p_0, and potential temperature θ can be used to quantify temperature changes along a Lagrangian air parcel trajectory. The incremental summation of temperature changes along a trajectory equates to the total temperature change of an air parcel ΔT. Following Hermann *et al.* (2020), and in agreement with Saigger and Gohm (2022), the integrated diabatic temperature change ΔT_{diab} in the time period $[t_{start}, t_{end}]$ is quantified by the summation of a numerical approximation of the second term on the right-hand side of Equation (1) using upstream finite differences and the average pressure between respective time steps ($dt = 10$ s):

$$\Delta T_{diab} = \sum_{t \in \{t_{start}+dt, \ldots, t_{end}\}} (\theta_t - \theta_{t-dt}) \left(\frac{2p_0}{p_t + p_{t-dt}}\right)^{-\kappa}. \quad (2)$$

The integrated adiabatic temperature change of an air parcel ΔT_{adiab} can then be quantified as the residual of the total temperature change and the diabatic temperature change[1]:

$$\Delta T_{adiab} = \Delta T - \Delta T_{diab}. \quad (3)$$

Equations 1–3 allow for a quantification of the total foehn air warming as well as for a separation of adiabatic and diabatic contributions. The heat budget framework is applied to each trajectory starting from the time instant it crosses the 50 km distance polygon (Figure 1b) to the moment when its latitude is closest to the latitude of the respective foehn location.

Additionally, in order to disentangle the net diabatic temperature change into the different diabatic processes (microphysical processes, subgrid-scale turbulence, radiative flux convergence), the retrieval of all diabatic temperature tendencies and the advection tendency is re-implemented into COSMO 5.6 based on older COSMO versions (Joos and Wernli, 2012; Papritz and Pfahl, 2016). Furthermore, in analogy to Miltenberger *et al.* (2016), temperature tendencies associated with phase changes (e.g., condensation of cloud droplets, evaporation of cloud and rain droplets) are explicitly retrieved from the microphysics scheme. The instantaneous Eulerian temperature tendencies are traced along the online trajectories and subsequently summed up to quantify the importance of the different diabatic processes for foehn air parcels:

$$\Delta T_{diab} = \sum_{t \in \{t_{start}+dt, \ldots, t_{end}\}} \left(\left.\frac{\partial T}{\partial t}\right|_{mphys} + \left.\frac{\partial T}{\partial t}\right|_{tur} + \left.\frac{\partial T}{\partial t}\right|_{rad} \right) \cdot dt + \Delta T_{residual}. \quad (4)$$

Although the temperature tendencies form a closed budget at each grid point in the interior model domain,

---

[1]We tested an explicit calculation of ΔT_{adiab} in analogy to Equation (2). The differences to the implicit calculation are negligible (on the order of 1×10^{-3} K). Hence, we prefer the aforementioned formulation, because Equation (3) is then perfectly closed.
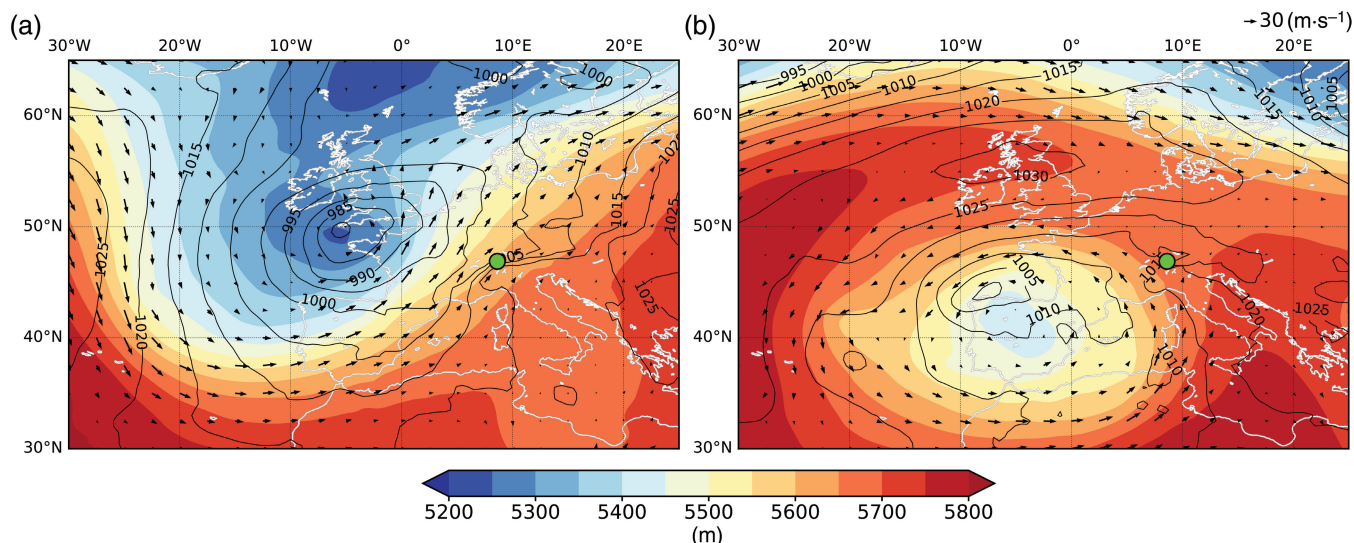
FIGURE 2 ERA5 geopotential height (in colours) and horizontal wind on 500 hPa and sea-level pressure (black contours) for (a) 1200 UTC November 21, 2016, and (b) 1200 UTC November 24, 2016. The position of Altdorf is marked with a green circle [Colour figure can be viewed at wileyonlinelibrary.com]

Equation (4) contains a residual term along the trajectories ($\Delta T_{\text{residual}}$). It is calculated as the difference between ΔT_{diab} from Equation (2) and the integrated diabatic tendencies in Equation (4). The residual can stem from several possible sources. First of all, as already illustrated by Miltenberger *et al.* (2016), potential temperature is not a perfectly conserved quantity in the COSMO model due to the non-conservative and diffusive formulation of the dynamical core. Second, to maintain a constant sample size during model integration, trajectories intersecting with the topography are artificially lifted to 10 m above the surface. This can introduce additional errors in the tendency budget. Third, Equation (4) assumes that the advective temperature tendency retrieved from COSMO corresponds to the actual temperature advection along an air parcel pathway, which might be violated due to interpolation and truncation errors in the trajectory calculation.

3 | SYNOPTIC- AND MESOSCALE CHARACTERISTICS

3.1 | Large- to Alpine-scale overview

In the course of November 19–21, 2016, an upper-level trough and its associated surface cyclone formed over the North Atlantic and subsequently approached Europe (Figure 2a). Prevailing southwesterlies and the upstream trough constitute an exemplary synoptic situation prone to south foehn formation in the Alpine region; for example, see Richner and Hächler (2013). In accordance with the large-scale situation, foehn breakthrough was observed in all major Alpine valleys on November 20.

During November 22 and 23, the trough remained quasi-stationary, thereby elongating and forming an upper-level cut-off low over the Iberian Peninsula. The cut-off persisted during the subsequent 2 days (Figure 2b), before finally splitting into two separate systems and ceasing the prolonged 6-day period of southerly flow in the Alpine region. The event ranked as the longest and second-longest uninterrupted foehn period since the start of automated measurements in Vaduz and Altdorf, respectively (Bader *et al.*, 2017). The longevity of the event is clearly linked to the characteristic synoptic situation. Usually, deep foehn events end with an abrupt breakdown due to the passage of a cold front (Sprenger *et al.*, 2016). In this case, however, upstream upper-level Rossby wave breaking and cut-off formation prevented the frontal propagation and enabled an exceptionally long-lasting foehn event.

As is often the case for south foehn events (Richner and Hächler, 2013), the case studied was accompanied by orographic precipitation on the windward slope of the Alpine chain. During both the first and the second 3-day period, local maxima exceeded 160 mm (Figure 3). Throughout the whole event, precipitation peaked at the western arc of the Alps along a band from Ticino (southern Switzerland) to the Maritime Alps. In contrast, intensity dropped strongly when moving eastward. The distribution corresponds to a typical pattern of orographic precipitation on the Alpine South side: When moist air from the Mediterranean approaches the Alps, the low-level inflow can be partially blocked and the curvature of the orographic obstacle induces an easterly barrier jet that redirects moisture towards the concavity (Rotunno and Houze, 2007; Schneidereit and Schär, 2000). Primary
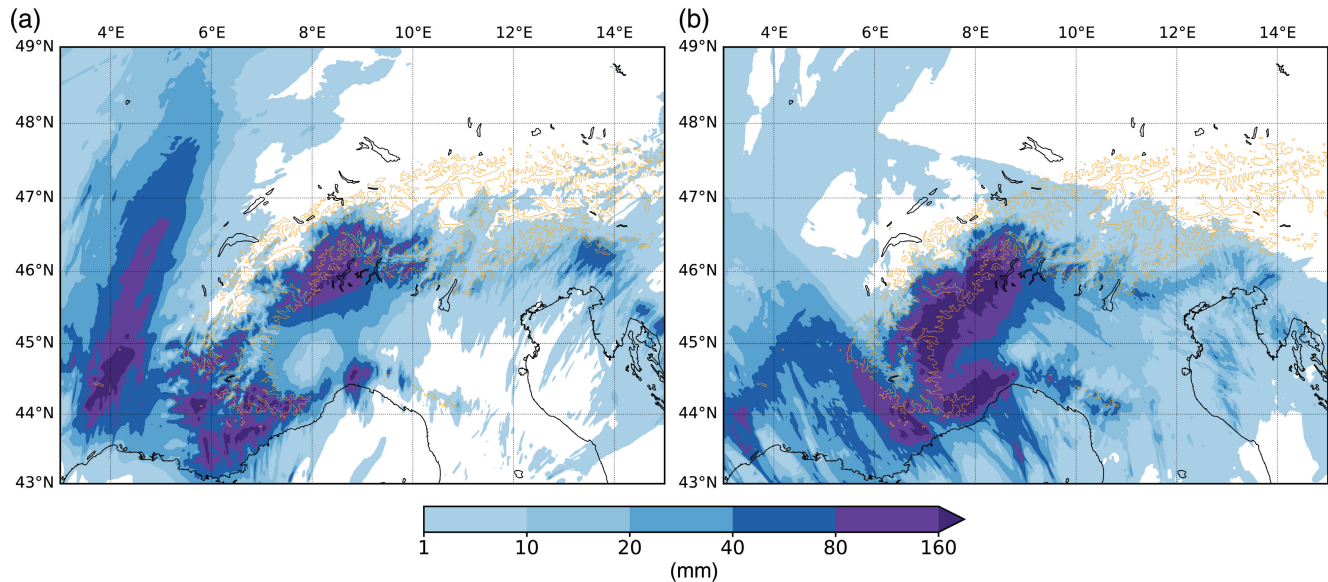
RMetS

FIGURE 3 Accumulated COSMO-1 precipitation during the event for (a) 1800 UTC November 19 to 1800 UTC November 22 and (b) 1800 UTC November 22 to 1800 UTC November 25. The 1,500 m contour of the topography is indicated by the orange line [Colour figure can be viewed at wileyonlinelibrary.com]

differences between the first and the second half of the event relate to the synoptic-scale flow evolution. During the first period, southwesterly to southerly flow leads to a precipitation maximum in the Lago Maggiore area and the Maritime Alps (Figure 3a). A frontal rain pattern is visible over France. As the event progresses, the precipitation maximum extends towards the whole western arc and, related to the southeasterly flow impinging on the Alps, the intensity increases (Figure 3b). The modelled precipitation pattern corresponds to reports on widespread floods in the southern Piedmont region (Nannoni *et al.*, 2020). It serves as a first indicator for the potential of intense diabatic heating of air parcels in the southerly inflow region.

3.2 | A detailed valley perspective

Changing the focus towards the northern side of the Alps, it is evident that the flow within the foehn valleys is governed by the large-scale flow conditions, but modified through local topography. Model-based pseudo-lidar plots from three valleys (Figure 4) demonstrate this relationship. The mid-tropospheric flow turns from a southwesterly to a southeasterly direction during the course of the event for all the valleys. Concurrently, south-easterlies prevail within the valley atmosphere of the Lower Valais (Figure 4a) and the Reuss Valley (Figure 4b), likely related to the orientation of the local valley axes and, in the case of the Reuss Valley, potentially also owing to the local outflow of the Schächen Valley (a tributary valley). During

the first 12 h of the event, downward-sloping isentropes indicate a deep warming. During mid November 20, the onset of the foehn close to the valley grounds can be observed, approximately matching the observed onsets (not shown). The foehn breakthrough induces a rapid growth of the boundary layer and reduces the static stability at low levels, corresponding to the turbulent nature of foehn flows. The onset is followed by the most intense phase of the event on November 21 and the first half of November 22, during which wind velocities peak and momentum mixes down to the surface (not shown). Afterwards, the mid-tropospheric flow weakens and maximum wind speeds are confined to the regions of contracted isentropes above the boundary layer. The final cessation on November 25 is accompanied by deep cooling. Besides the common overall evolution, some notable differences between these three valleys exist: Whereas the maximum wind velocities in the Reuss and the Rhine Valley (Figure 4b,c) extend throughout the entire boundary layer, peak winds are mostly restricted to the boundary layer top in the Lower Valais (Figure 4a). Furthermore, the region of maximum wind speeds propagates upward during the event in the Lower Valais. Finally, a short reintensification is observed during November 24, yet this finding is mainly restricted to the Reuss and the Rhine Valley.

The distinct evolution in foehn intensity (discernible as varying wind velocities in Figure 4) is clearly linked to the temporal evolution of the cross-Alpine geopotential height difference on 850 hPa between Lugano (8.95°E, 46.00°N) and Kloten (8.54°E, 47.48°N) as depicted in Figure 5. The difference increases rapidly during the first 12 hr of
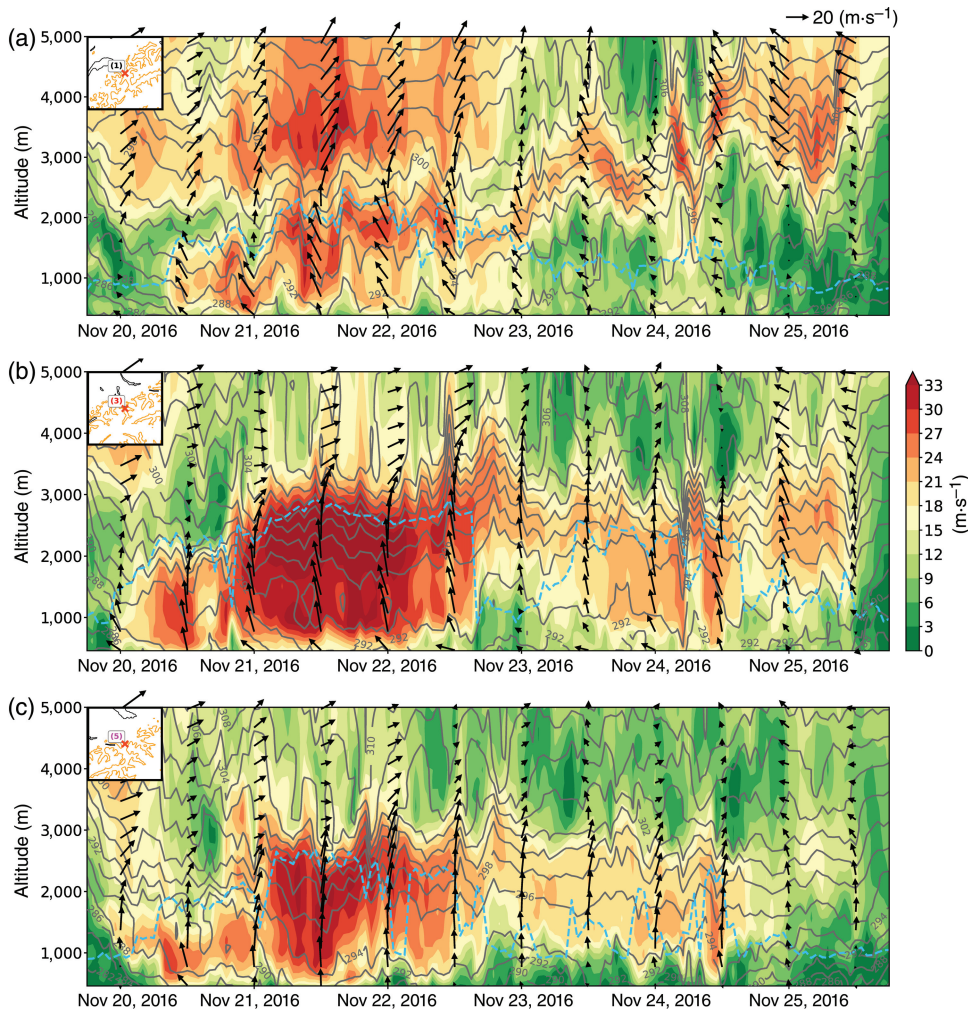
FIGURE 4 COSMO-based lidar plots of the horizontal velocity field (colour and vectors; the wind vectors indicate wind direction and speed in the horizontal plane) and potential temperature (grey contours) as well as the height of the boundary layer (sky blue) are shown for (a) Lower Valais, (b) Reuss Valley, and (c) Rhine Valley. The exact locations used for the lidar plots are specified in Table 1 [Colour figure can be viewed at wileyonlinelibrary.com]

the event and peaks on November 21. The maximum is followed by a subsequent decrease and a minor reintensification on November 24, before the difference drops to near-zero values on November 25. The link between foehn intensity and the cross-Alpine pressure gradient is well known among forecasters (Gerstgrasser, 2017) and has been mentioned in earlier publications as well (Sprenger *et al.*, 2017). Figure 5, however, points out that this relation can be expanded to the Lagrangian air parcel perspective: The number of air parcels arriving within the foehn valleys exhibits a considerable co-variability with respect to the cross-Alpine geopotential height gradient (mean Pearson correlation of 0.62). An elevated flow velocity leads to a larger volume of air being transported through the valleys per time, which reflects in a larger number of air parcels passing by (see Figures 4 and 5). It is a striking feature that the number of trajectories arriving within the foehn valleys only increases with a time lag of ~18 hr on November 20. Potentially, this time lag is caused by the residual cold-air pools within the different valleys (see also Figure 4), which need to be eroded prior to foehn breakthrough at the valley floor. However, it is probably

further amplified, since air parcels require a certain time span to arrive within the foehn valleys after being released upwind, whereby the trajectory set-up inherently introduces a certain time lag. Having established the synoptic- and mesoscale flow evolution and its linkage to the air parcel transport, the study will now focus on the foehn air warming during the event using the Lagrangian heat budget methodology (Section 2.3).

4 | LAGRANGIAN HEAT BUDGET

4.1 | The heat budget methodology: An illustrative example

The goal of the heat budget is to assess the magnitude and the temporal evolution of both the net foehn air warming and its contributing processes, including adiabatic contraction/expansion, cloud microphysical processes, turbulent mixing, and radiation. The theoretical framework of the heat budget methodology was introduced in Section 2.3. Here, a practical example is presented first. Figure 6a shows a subset of trajectories arriving in the
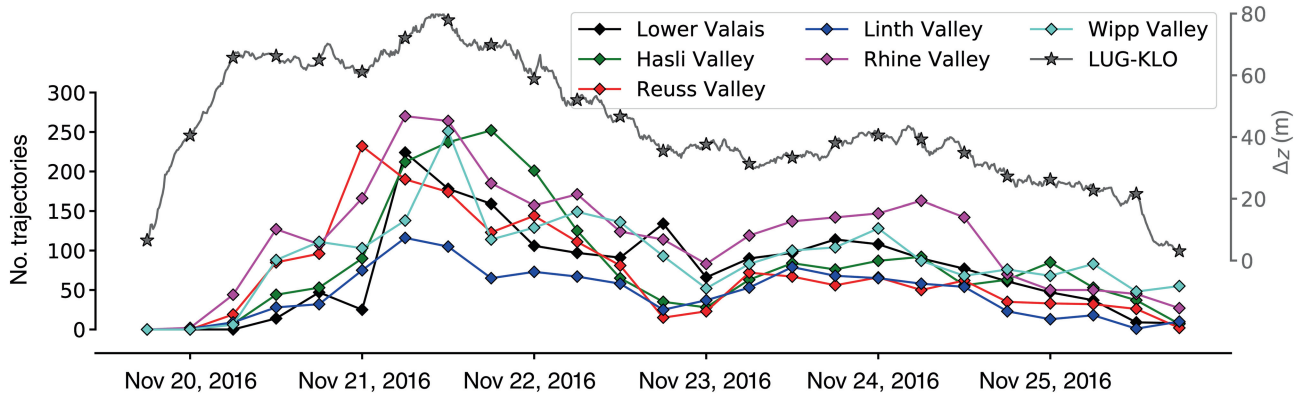
FIGURE 5 Time series of the geopotential height difference on 850 hPa between Lugano and Kloten (grey, star markers) and the number of trajectories arriving within the six valleys (coloured, diamond markers). The number of trajectories is binned in six-hourly windows [Colour figure can be viewed at wileyonlinelibrary.com]
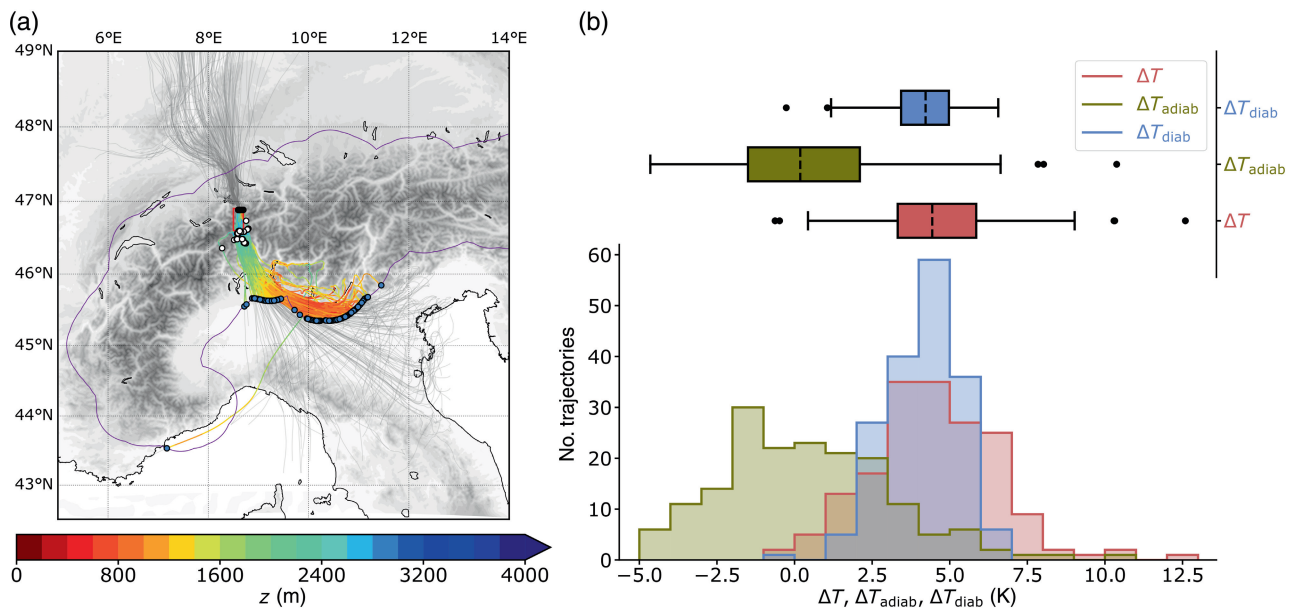

FIGURE 6 Illustrative example of trajectories and heat budget terms. (a) Trajectories arriving in the Reuss Valley in a six-hourly time window centred around 1200 UTC November 21, 2016. The upstream reference points (blue), crest points (white), and valley reference points (black) are marked and the 50 km polygon is shown (violet). The coloured segments of the trajectories correspond to the segments considered for the heat budget. An enlarged version of this figure can be found in the supplement (Figure S2). (b) The distribution and box plots of ΔT, ΔT_{adiab}, and ΔT_{diab} for this specific subsample of trajectories [Colour figure can be viewed at wileyonlinelibrary.com]

Reuss Valley in a six-hourly time window centred around 1200 UTC on November 21. To have a consistent upstream reference point for all trajectories and valleys, the 50 km distance polygon around the Alps (see Figure 1b) is again considered. The integration of the heat budget for each trajectory is initialised (t_{start}) at the time the trajectory intersects with the polygon for the first time. It then continues until the trajectory is located within the valley bounding box and has reached the latitude closest to the foehn location (t_{end}). In Section 4.3, the diabatic processes will be split into upstream and downstream contributions.

The dividing crest position along a trajectory is defined as the time instant the air parcel passes the highest topography beneath. Having defined the integration window for the heat budget (see also coloured segments in Figure 6a), the net warming and both the adiabatic and the diabatic contributions according to Equations 1–3 for this specific subset of trajectories can be quantified as displayed in Figure 6b: Most trajectories experience a net warming governed by diabatic heating, whereas the adiabatic temperature change is negligible in the median, although exhibiting a considerable spread. In the following, the heat
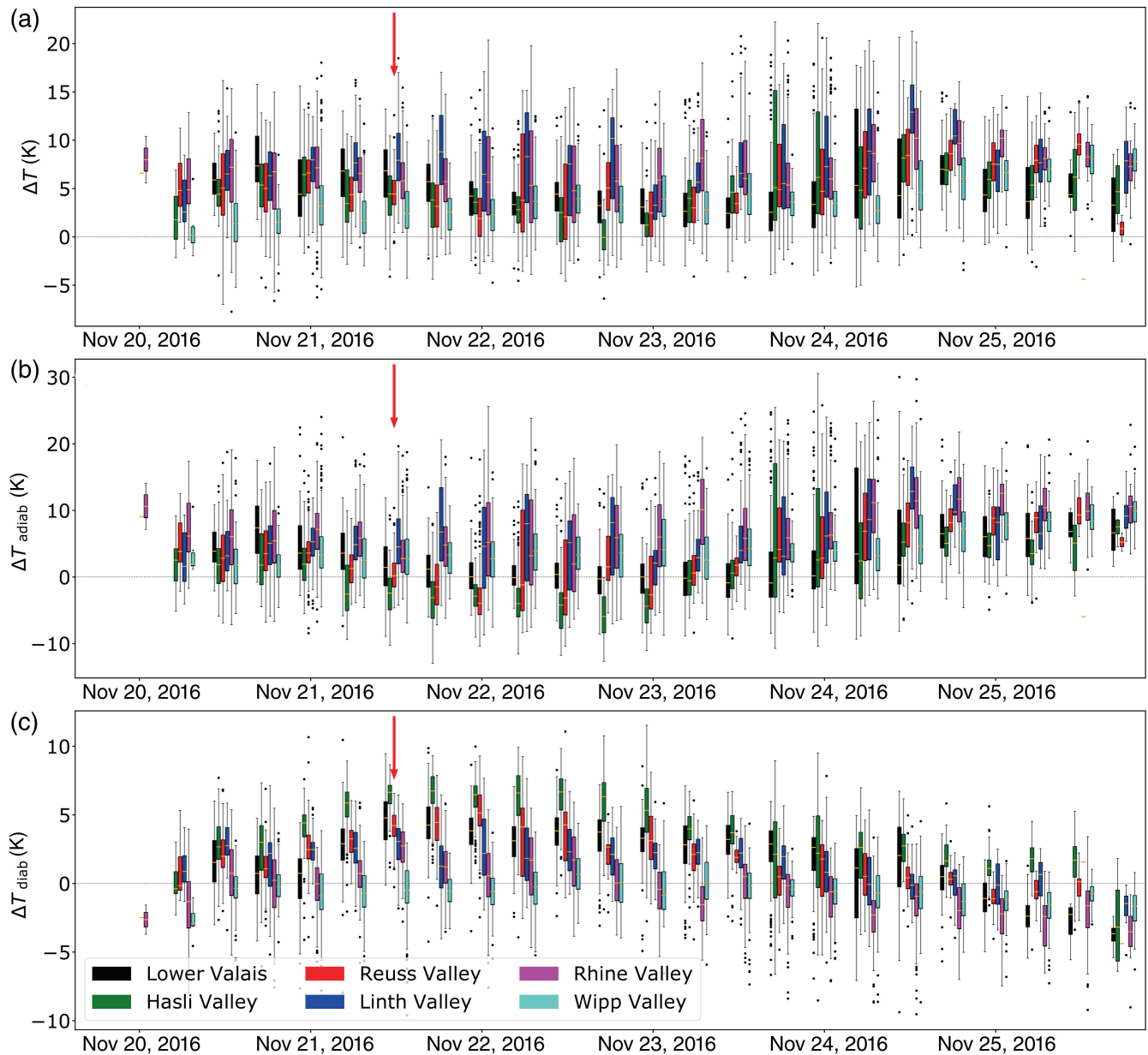
FIGURE 7 Temporal evolution of the Lagrangian heat budget terms for the six different valleys displayed in six-hourly bins. (a) Total temperature change ΔT; (b) adiabatic temperature change ΔT_{adiab}; (c) diabatic temperature change ΔT_{diab}. The red arrows mark the box plots for the Reuss Valley at 1200 UTC on November 21, 2016, that were shown in Figure 6 [Colour figure can be viewed at wileyonlinelibrary.com]

budget methodology will be applied to all six-hourly time windows for the six different Alpine valleys considered in this study.

4.2 | Magnitude and temporal evolution of the warming mechanisms

The net temperature change along trajectories agrees with the traditional Eulerian perspective on foehn air warming (Figure 7a): Air parcels predominantly experience a net warming along their pathway for all valleys (overall 92.6%). The warming has a characteristic magnitude of ~ 5 K, but the variability between distinct air parcels is considerable and ranges from an overall cooling to warming with a magnitude larger than 15 K. The six different Alpine valleys share a common temporal evolution that can be divided into three time periods (see also Figure S3 showing the medians to highlight the temporal evolution). At first, the foehn air warming is elevated during November 20 and 21. During the subsequent 2 days, the magnitude is slightly reduced before it recovers again on the evening of November 23, while the intra-valley variability increases as well. The overall strongest warming is
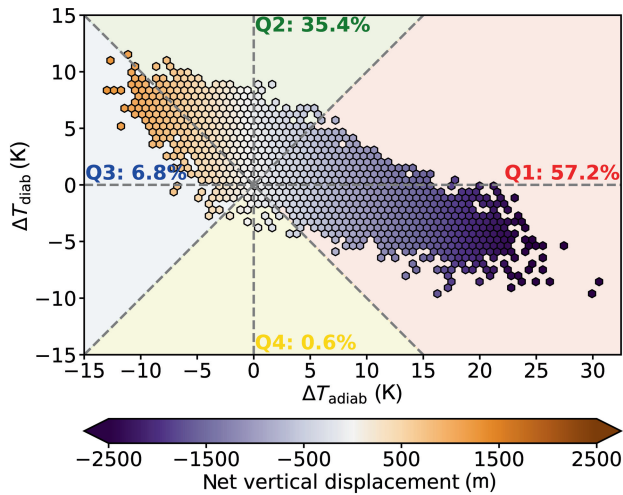
RMetS

FIGURE 8 Relation between adiabatic and diabatic temperature change coloured by the net vertical displacement for all trajectories and all valleys in a binned histogram. Q1–Q4 refer to the four quadrants (coloured areas) spanned by the diagonals. Q1 (red): warming dominated by adiabatic heating; Q2 (green): warming dominated by diabatic heating; Q3 (blue): cooling dominated by adiabatic cooling; Q4 (yellow): cooling dominated by diabatic cooling [Colour figure can be viewed at wileyonlinelibrary.com]

diagnosed on November 24. The Wipp Valley deviates from the consistent evolution among the valleys in terms of a reduced magnitude, but it shares a similar temporal evolution to the other valleys. The reduction in warming during November 22 and 23 is more pronounced for the western Alpine valleys, especially in Lower Valais and Hasli Valley.

The adiabatic temperature change (Figure 7b) resembles the temporal evolution of the net contribution and supports the trisection of the event: An enhanced adiabatic warming period is followed by a reduction and a subsequent re-enhancement. This finding agrees with Miltenberger *et al.* (2016), where they point out the predominance of adiabatic warming for the overall heat budget. There is, however, a pronounced contrast between western and eastern Alpine valleys during the central phase of the event that was not discussed by Miltenberger *et al.* (2016) because of their restriction to a single valley (Rhine Valley): Whereas the eastern valleys experience a slight (Rhine Valley and Linth Valley) or no decrease (Wipp Valley) in adiabatic warming, the contribution drops considerably for the western valleys (Lower Valais, Hasli Valley, and Reuss Valley), thereby reaching negative values. These trajectories thus experience adiabatic cooling, which can be explained upon considering their original altitude over the Po Valley. They stem from lower levels compared with their arrival altitude within the foehn valleys (see also hexagons with $\Delta T_{\text{adiab}} < 0$ in Figure 8).

Focusing on the diabatic temperature change (Figure 7c), it is evident that the contribution is

anti-correlated to the net change and the adiabatic component. This results in a rather complex combined effect of both heat budget terms. If the diabatic temperature change is of opposite sign to the adiabatic temperature change, the magnitude of the net temperature change is reduced, otherwise it is magnified. At first, the diabatic heating ranges at ∼2 K for all valleys. Afterwards, the inter-valley spread is strongly enhanced: The eastern Alpine valleys experience almost no increase in diabatic heating, whereas a pronounced increase to ∼5 K is observed for the western Alpine valleys. This striking contrast between the two valley categories provides an explanation for the evolution of the net warming during the central phase of the event. Air parcels of the western valleys experience an adiabatic cooling due to net ascent, but the cooling is overcompensated by diabatic warming, resulting in a reduced, yet positive, net warming (see hexagons in Q2 with $\Delta T_{\text{adiab}} < 0$ in Figure 8). Later, the contrast between the valleys shrinks and the overall diabatic contribution drops to predominantly negative values during the last 1.5 days. The findings partly agree with the moist foehn case in Miltenberger *et al.* (2016), but some important differences need to be pointed out: Whereas Miltenberger *et al.* (2016) only observed a warming for ∼50% of the foehn trajectories, we register a warming for the vast majority of air parcels. The overall importance of the adiabatic and the diabatic temperature change for the Rhine Valley quantified according to the formulation in Miltenberger *et al.* (2016) is comparable (72.8% in the 2016 event versus ∼70% in the 2013 moist case), but we observe a more accentuated temporal evolution. In particular, the comparison of major Alpine valleys reveals pronounced differences between them: Whereas the warming in eastern Alpine valleys is driven by adiabatic contraction, the heat budget of the western Alpine valleys experiences considerable modulation by diabatic processes during the most intense phase of the foehn event.

The two-dimensional phase space spanned by the adiabatic and diabatic temperature change of all trajectories in the six valleys (Figure 8) helps to summarise the key findings related to the net heat budget as follows: Most of the air parcels experience a net warming (Q1 + Q2 sum up to 92.6%). The majority of air parcels (Q2: 57.2%) are mainly warmed by adiabatic descent, although a considerable fraction of the warming (Q2: 35.4%) is driven by diabatic processes. The adiabatic temperature change is essentially governed by the sign and magnitude of the cross-Alpine net vertical displacement of air parcels: Most trajectories experience a negative net vertical displacement, pointing out their elevated origin over the Po Valley before descending along strongly sloping isentropes downstream of the crest (isentropic drawdown mechanism). A smaller fraction of air parcels experiences adiabatic cooling related

to their positive net vertical displacement, hence their low-level upstream sourcing. Oftentimes, these trajectories are subject to intense diabatic heating, which sometimes exceeds the adiabatic cooling and results in net warming (hexagons in Q2 with $\Delta T_{\text{adiab}} < 0$). The small fraction of cooled air parcels is, to a large extent, cooled by adiabatic ascent (Q3: 6.8%), while a minor share is exposed to net cooling due to diabatic processes (Q4: 0.6%). The anti-correlation of the adiabatic and diabatic temperature change prevents the occurrence of extreme net temperature changes, as both extreme adiabatic and diabatic heating are likewise dampened by the other respective process of opposite sign. Consequently, the spread of the net temperature change (-8 to 22 K) is smaller than the spread of the adiabatic temperature change (-13 to 31 K).

4.3 | Upstream and downstream diabatic processes

The previous section revealed a considerable effect of diabatic processes on the heat budget of the foehn trajectories. Accordingly, in a next step, the diabatic heating and cooling are disentangled into the possible mechanisms to gain further insight into the thermodynamics of the event. The net effect of the different processes for all six valleys is shown in Figure 9, whereas each process is further subdivided into an upstream (i.e., before crest) contribution and its downstream counterpart. This adds spatial information to the heat budget.

The net diabatic contribution (black boxes) resembles the pattern previously observed in Figure 8c: The magnitude is larger for the western valleys, peaking for the Hasli Valley (~5 K), and then continuously drops as the focus shifts eastward. The net diabatic effect nearly vanishes (~0 K) for the Rhine Valley and becomes negative for the Wipp Valley. As a consistent pattern for all valleys, the net diabatic change is composed of a larger upstream diabatic warming (black boxes with dashed edges) that exceeds the net effect by ~1–3 K and a corresponding diabatic cooling between crest and the different foehn valleys.

Focusing on the upstream side, it is evident that the upstream diabatic heating is almost entirely caused by upstream latent heating in clouds (essentially condensation—see Figure S4) for all valleys. Turbulence does not induce any net diabatic effect, although individual trajectories experience turbulent cooling or warming on the upstream side of the Alps. Radiation is mostly unimportant for this particular foehn case except for the Rhine Valley (where minor contributions of long-wave cooling emerge) and for the Wipp Valley (where small contributions by short-wave heating and long-wave cooling modulate the diabatic heat budget).

Downstream of the Alpine crest, diabatic cooling of air parcels is induced by two different processes. The slightly more important (~0.7–1.4 K) contribution is again related to cloud microphysical processes: During the descent into a foehn valley, cloud and rain droplets in an air parcel start to evaporate (Figure S4) as it is warmed by adiabatic contraction, thereby leading to diabatic cooling.[2] The second driver for the diabatic cooling stems from turbulent mixing (~0.3–0.8 K). The identified effect of turbulence in this study is seemingly opposed to an earlier finding from Elvidge and Renfrew (2016). However, it depends upon the exact arrival altitude and position of individual air parcels that are considered whether they experience turbulent heating or cooling. In a stably stratified atmosphere, mechanical downward mixing is expected to increase potential temperature along a foehn valley (Seibert, 1985). However, the exact effect of turbulent mixing, as indicated by the simulation, is rather heterogeneous. Furthermore, the temperature tendencies due to turbulence and advection are mostly compensating each other, resulting in a net effect that is usually much smaller (similar to Umek et al., 2021; not shown). More comprehensively assessing the turbulence effect on the temperature evolution of the near-surface air in the foehn valleys would require a detailed Eulerian heat budget analysis, which is beyond the scope of this study. In summary, evaporative cooling and turbulent mixing together explain the diabatic cooling of air parcels during their descent.

Although the heat budget contains all diabatic processes that potentially affect an air parcel, there still exists a residual. The median of the residual is close to zero for all foehn valleys (largest deviation of -0.3 K for the Lower Valais), but it tends to be slightly negative overall. This might indicate that our method overestimates upstream diabatic heating or underestimates downstream turbulent cooling or evaporative cooling. Since the residual is smallest for the Hasli Valley, where cloud microphysical processes dominate both the upstream and the downstream components of the heat budget, the residual is likely caused by an underestimation of the turbulent cooling effect. Downstream turbulence is also the driver for the unrealistic outliers of some trajectories. They are related to trajectories very close to the surface, where the advective temperature tendency and the turbulence

---

[2]Seibert (1985) highlighted that the evaporative cooling of cloud droplets in the lee completely compensates the upstream latent heating if an air parcel does not precipitate and interpreted it as an argument against the applicability of the thermodynamic foehn theory in the Austrian Alps. Indeed, we can confirm that most of the upstream heating is compensated by downstream cooling for the Austrian Wipp Valley. However, the compensational effect shrinks for the western valleys, where air parcels experience stronger rainout during their Alpine crossing.
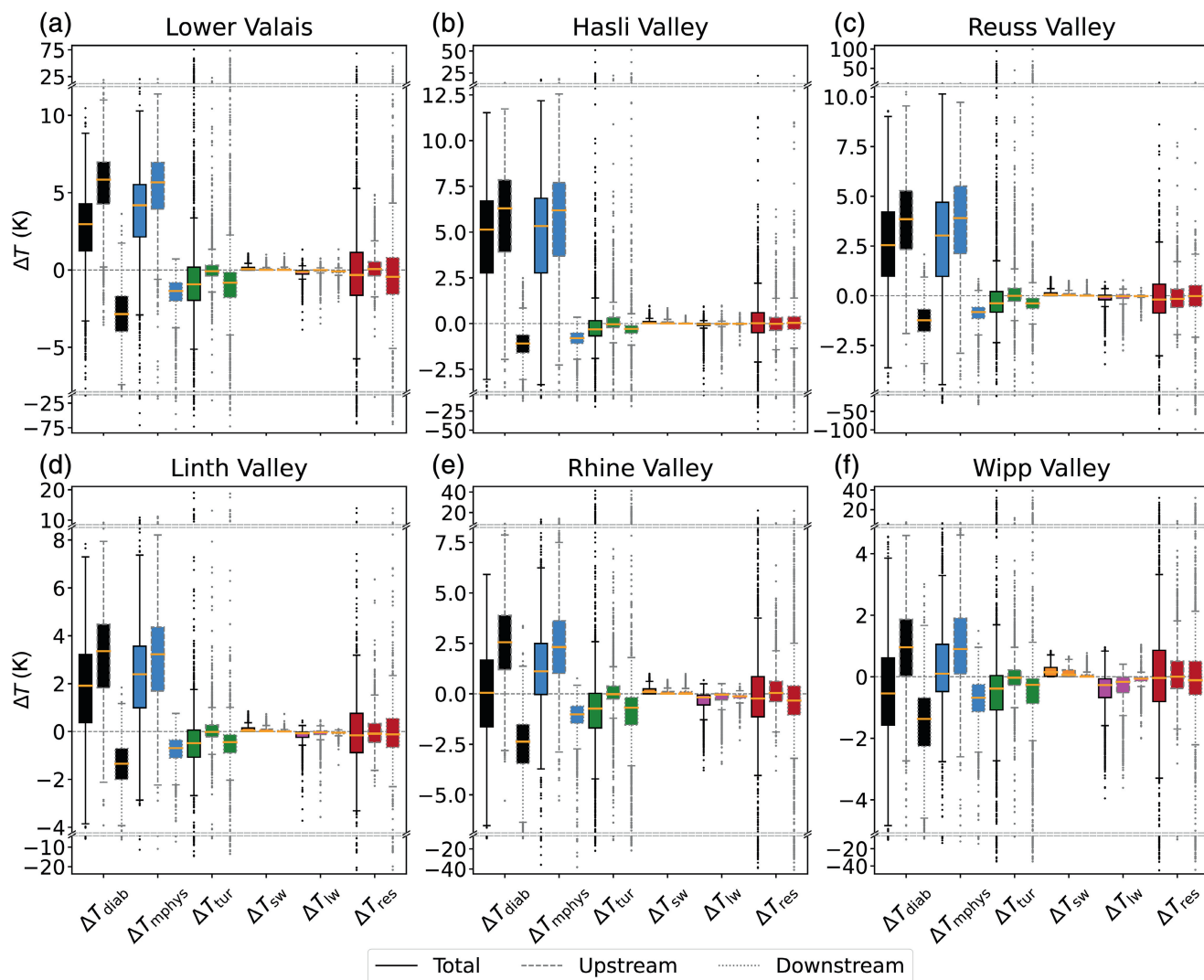
FIGURE 9   Accumulated diabatic temperature tendencies along trajectories (see Section 2.3 for technical details) for the six different valleys. Colours indicate the different diabatic processes. For each process, three boxes are displayed showing the total temperature change (left; solid whiskers), the upstream temperature change (centre; dashed whiskers), and the downstream temperature change (right; dotted whiskers) [Colour figure can be viewed at wileyonlinelibrary.com]

tendency both reach high numbers and strongly compensate each other in the model, leading to unrealistic overestimations of turbulent cooling and heating effects. For an additional discussion regarding the residual term, the reader is referred to Section 2.3.

Despite the outliers and the slightly negative residual, we are confident to deduce several key findings from the diabatic tendency budget. First, foehn trajectories in all valleys experience upstream diabatic heating and downstream diabatic cooling, which again agrees with Miltenberger *et al.* (2016). We identify condensation in clouds as the main driver for upstream latent heating. Second, the downstream diabatic cooling is driven by two different processes: Both evaporation of rain and cloud droplets and turbulent mixing tend to

induce diabatic cooling during the descent of foehn air parcels.

5 | THERMODYNAMIC AIRSTREAMS

5.1 | Definition and differences between valleys

The previous section revealed a strong spread in the adiabatic and diabatic warming contributions towards the net heat budget for the different valleys. Next, the aim is to relate this spread to the potentially different pathways that air parcels undergo between the upstream Po Valley and
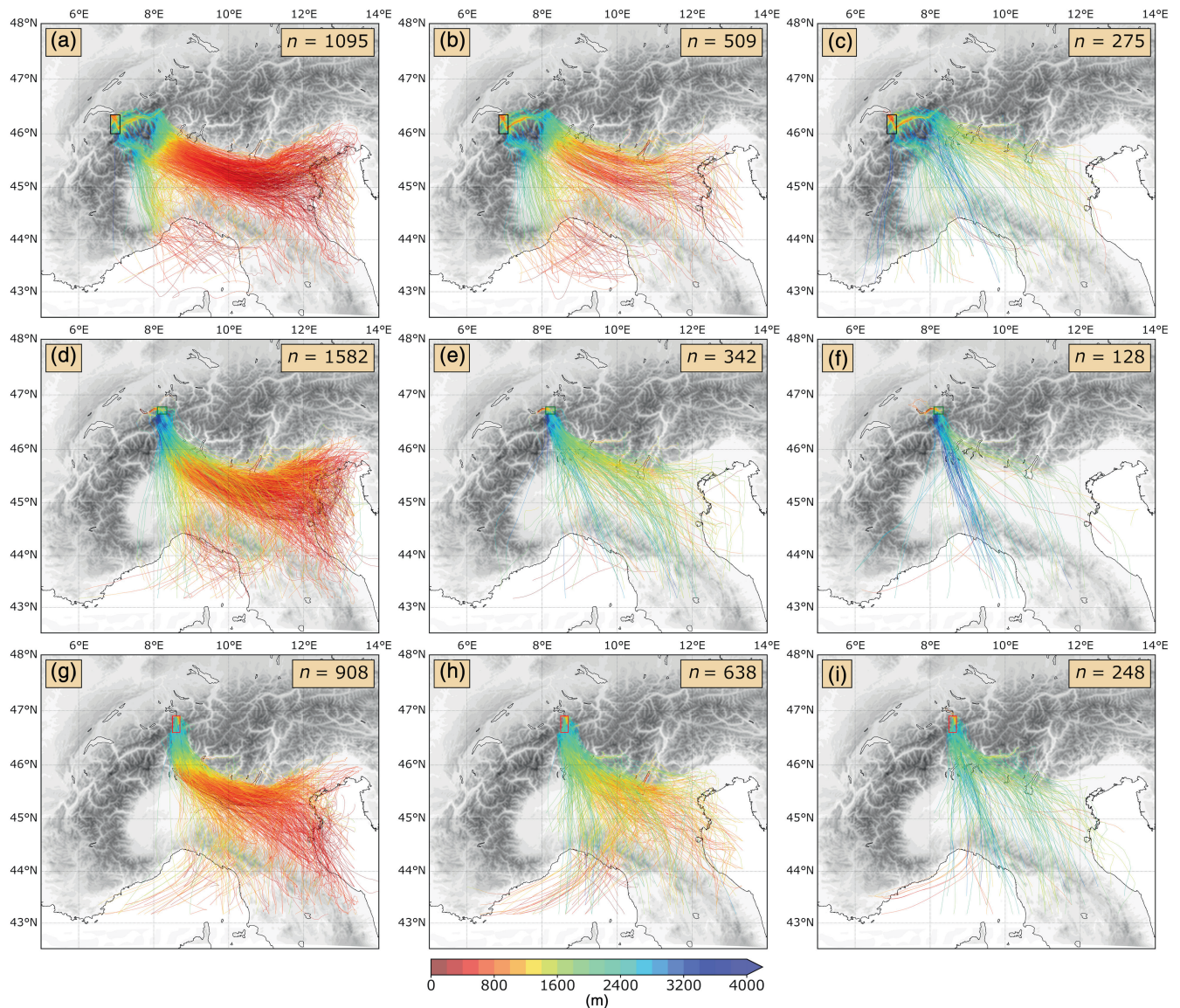
FIGURE 10 Thermodynamic trajectory classifications for (a)–(c) the Lower Valais, (d)–(f) the Hasli Valley, and (g)–(i) the Reuss Valley. Strongly heated airstream: right column; weakly heated airstream: centre column; cooled airstream: left column. The number of trajectories *n* within each category and for each valley is given in the upper right corner [Colour figure can be viewed at wileyonlinelibrary.com]

their descent into the foehn valleys. To this end, a simple criterion based on the integrated diabatic temperature change ΔT_{diab} is applied to distribute the trajectories into three categories as follows:

- trajectories with $\Delta T_{\mathrm{diab}} \geq 2.5$ K, strongly heated airstream (SHAS);
- trajectories with 0 K $\leq \Delta T_{\mathrm{diab}} < 2.5$ K, weakly heated airstream (WHAS);
- trajectories with $\Delta T_{\mathrm{diab}} < 0$ K, cooled airstream (CAS).

The resulting trajectory clusters are shown in Figures 10 and 11 for the western and eastern Alpine valleys, respectively. A striking feature is the pronounced

contrast in position and altitude of origin between the three categories for the different valleys. SHAS trajectories (e.g., Figure 11a) predominantly originate in the eastern Po Valley at low levels. Subsequently, easterly winds gather these air parcels before they ascend and cross the Alps. SHAS reveals the presence of near-surface easterlies in the Po Valley related to the low-level flow blocking, as it is often observed when synoptic-scale southerly flow approaches the Alps (Rotunno and Houze, 2007; Schneidereit and Schär, 2000). A small number of air parcels within the SHAS category originate over the Gulf of Genua and are advected with the southwesterly flow before they are integrated into the low-level barrier jet structure. The Lower Valais (Figure 11a) stands out,

since some of its marine trajectories do not join the Po Valley airstream but ascend as soon as they make landfall, whereat they cross the Alps through the inlet of the Great St Bernard Pass. This ascent is likely caused by orographic lifting along the southeastern foothills of the Maritime Alps and potentially supported by convective activity along the Ligurian coastline (especially on the evening of November 20; not shown). During their strong ascent, SHAS trajectories experience intense diabatic heating. In agreement with the overall reduced diabatic heating in the eastern Alpine valleys (see Figure 9), the number of trajectories within this category drops substantially for the eastern valleys (Figure 11a,d,g), whereas it constitutes the overall most important airstream for western valleys (Figure 10a,d,g).

CAS contrasts the SHAS airstream: The majority of air parcels originate at a more southerly location and at substantially higher levels (e.g., Figure 11c). These air parcels get advected quasi-horizontally without deflection by orographic flow blocking during their approach of the Alps, before descending in the lee. Owing to the small upstream ascent, CAS trajectories experience reduced upstream diabatic heating. Overall, these air parcels are cooled diabatically when they arrive within the foehn valleys.

The WHAS airstream represents a mixture between the other two categories, both in terms of altitude and also origin of air parcels (e.g., Figure 11b). Some of the WHAS trajectories also tend to curve anticyclonically, but they approach the Alps at a higher level compared with the low-level SHAS trajectories. The Lower Valais, again, stands out, since WHAS air parcels also originate at near-surface altitudes (Figure 10b). Potentially, low-level air parcels that do not experience intense diabatic heating are subject to forced orographic lifting in the concavity close to Lago Maggiore and, therefore, enabled to cross the Alpine barrier into the Valais region.

Overall, the categorisation reveals a strong linkage between the pathway of foehn air parcels and their thermodynamic history: Low-level trajectories experience orographic blocking and are preferentially redirected towards the Alpine concavity. They need to ascend more strongly, thereby experiencing enhanced latent heating. In contrast, trajectories from higher levels approach the Alps in a more linear pathway due to the absence of orographic blocking at higher levels. They experience little diabatic heating or diabatic cooling during their progress. SHAS resembles the "Swiss foehn type", whereas CAS indicates an "Austrian foehn type" (Steinacker, 2006; Würsch and Sprenger, 2015). The concurrent consideration of a range of Alpine valleys reveals that these archetypes exist in the west and east Alps, whereas, in between, a continuous transition with a mixed-type variant is discernible (WHAS). Having established the linkage of air parcel thermodynamics

and distinct airstreams, as well as the importance of the airstreams for the different valleys, the next sections will analyse their temporal evolution in the context of the overall event evolution (Section 5.2) and their characteristic cloud and precipitation pattern, as well as the differential ascent and descent behaviour (Section 5.3).

5.2 | Temporal evolution of airstreams

Upon consideration of the three-phase evolution of the net diabatic temperature change (ΔT_{diab}; see Section 4.2), it can be anticipated that the dominant occurrence of the three air-stream categories is limited to specific time periods of the event. To illustrate this, Figure 12 depicts the relative fraction of trajectories belonging to the different categories in six-hourly time steps. Indeed, SHAS trajectories (Figure 12a) are the dominating contributor to foehn air parcels for the western Alpine valleys from November 21 until mid November 23. Peak values of virtually 100% are reached for the Hasli Valley during this period. On the other hand, SHAS contributes 20–60% to the foehn air parcels arriving within the Linth and the Rhine valleys. For the Wipp Valley, this airstream is no relevant contributor to the foehn flow (contribution always <20%). It should be emphasised that the important period of SHAS coincides with the peak in the total number of trajectories arriving within the foehn valleys (see Figure 5), which underlines the significance of this airstream for the most intense time period of the event and explains the enhancement in diabatic heating for the western valleys during November 21–23 (Figure 9c). Accordingly, the SHAS contribution is reduced during November 20 and 24–25, when the total number of trajectories is smaller.

CAS exhibits an anticorrelated evolution to SHAS: During the first 6 hr, it constitutes the dominating airstream. This demonstrates the fact that, at first, foehn air parcels approach the Alps close to crest level and are advected quasi-horizontally prior to their descent. During the central period, CAS is unimportant except for the Rhine Valley and the Wipp Valley, which exhibit "Austrian foehn type" characteristics throughout the whole event. During November 24–25 , CAS trajectories dominate the overall budget and contribute most strongly to the foehn flow. The maxima in CAS importance match with the time periods when the overall warming is driven by the adiabatic contribution (Figure 8), highlighting its importance for the foehn air warming during the beginning and the last phase of the event.

WHAS trajectories represent a mixed type between the two boundary categories (SHAS and CAS). Consequently, WHAS does not exhibit a distinct temporal evolution (Figure 12b). Its contribution ranges from
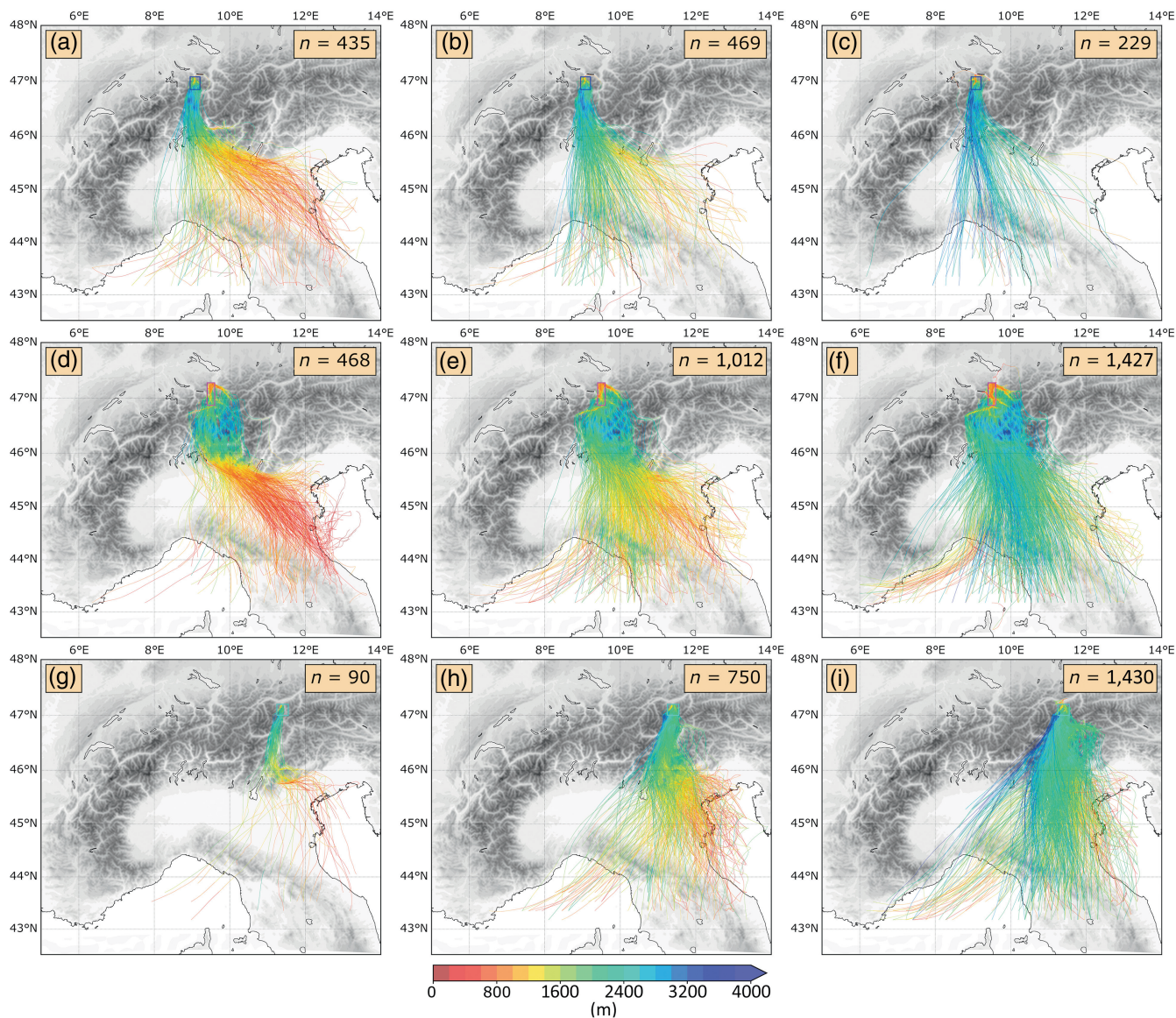
FIGURE 11 Same as Figure 10, but for (a)–(c) the Linth Valley, (d)–(f) the Rhine Valley, and (g)–(i) the Wipp Valley [Colour figure can be viewed at wileyonlinelibrary.com]

20 to 60% during the first 5 days of the foehn event, except for the Hasli Valley, where values rapidly drop. During the last day, WHAS contributes most of the foehn air parcels to the Linth Valley and Hasli Valley, whereas the importance tends to decrease for the other valleys.

The distinct temporal evolution points out that we not only observe the typical transition from more "Swiss foehn type" to "Austrian foehn type" when moving from the western to the eastern valleys, but the same transition is also observed over time. Indeed, at first, trajectories are advected quasi-horizontally towards the Alpine crest, and only afterwards, along with the event intensification, air parcels from lower levels are able to ascend over the Po Valley. Finally, during the last phase, foehn air parcels

again stem from elevated upstream source regions, as it is typical for the "Austrian foehn type".

5.3 | Linkage to cloud and precipitation pattern

Having found a clear linkage between the temporal evolution of the foehn air warming and the respective airstreams, this last section aims at analysing the spatial pattern of cloud and precipitation formation as well as the major diabatic tendencies (condensation, evaporation, turbulence) during the upstream ascent and subsequent descent. To this end, each trajectory is subdivided into an upstream and a downstream fragment separated by its

FIGURE 12 Temporal evolution of the relative fraction (%) of the different air-stream categories: (a) SHAS; (b) WHAS; (c) CAS [Colour figure can be viewed at wileyonlinelibrary.com]
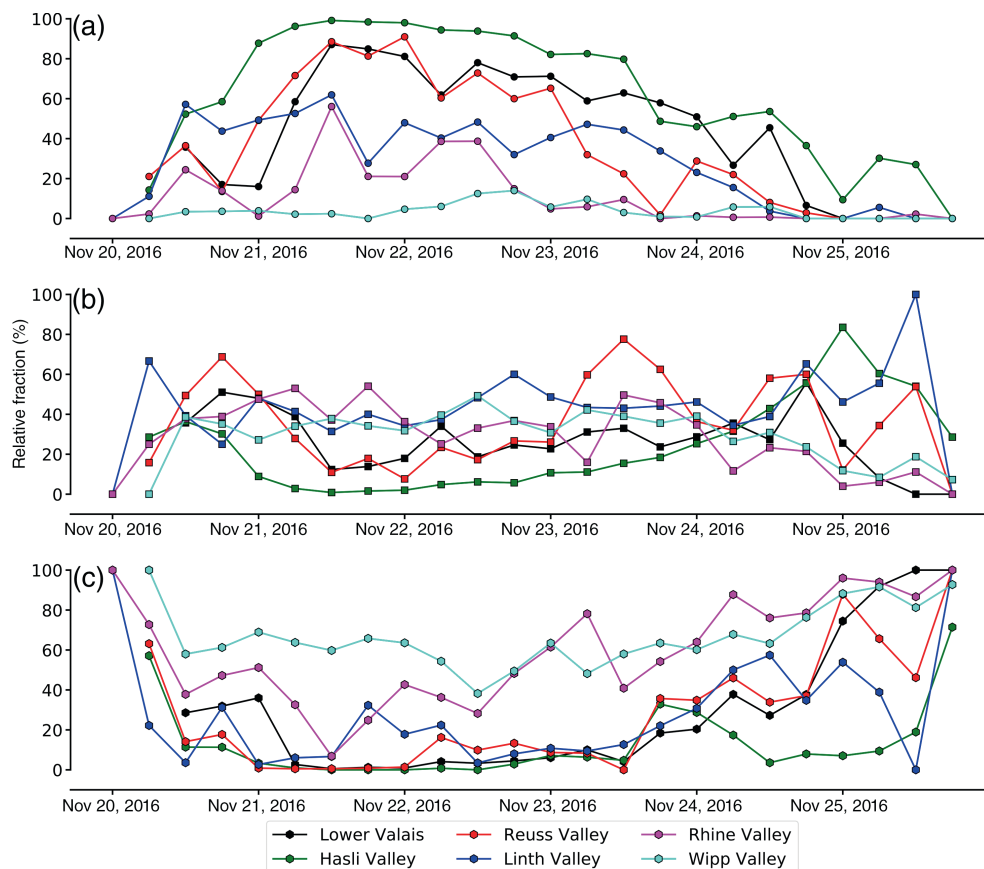
crest point, whereas both fragments are normalised to a common time axis by linear interpolation.[3] Then, a lidar scan using the 10-min resolved three-dimensional fields is created along all trajectories. Mean lidar scans of SHAS (left column) and CAS trajectories (right column) are shown in Figure 13a,b for the Lower Valais, Figure 13c,d for the Reuss Valley, and Figure 13e,f for the Rhine Valley.

SHAS air parcels ascend cross-isentropically from a common altitude of ~1 km to the crest level. During their ascent, they are subject to intense cloud and rain water formation within the atmospheric column of the lowest 4 km. SHAS trajectories tend to pass just below the region of maximum cloud water and ice, while their pathway is still above the maximum in precipitating hydrometeors during the crest approach. Both maxima are located further upstream for the Lower Valais, whereas they are more closely bound to the southern foothills of the Alps for the

Reuss Valley and the Rhine Valley. The spatial cloud distribution largely corresponds to the areas where condensational heating is enhanced (yellow contours in Figure 13). Trajectories tend to ascend at the lower edge of the condensational heating maximum in clouds. Potentially, this can be explained invoking a buoyancy argumentation, similar to Smith *et al.* (2003): Along the diagnosed ascent pathway, trajectories experience just enough condensational heating to ascend cross-isentropically to the crest, while their buoyancy still allows for a steep downstream descent. Air parcels travelling further aloft this ascent pathway might be subject to additional latent heating and, hence, are too positively buoyant to descend to near-surface levels downstream of the crest. This finding also implies the absence of air parcel scrambling as identified by Smith *et al.* (2003) and Miltenberger *et al.* (2016) in their respective case studies. At the same time, trajectories below the ascent pathway need to pass through the maximum in precipitating hydrometeors, which tend to hinder efficient ascent by increasing the density of air parcels and inducing evaporative cooling when rain droplets fall into unsaturated regions. Accordingly, in the near-surface region of the southern Alpine valleys, a downvalley circulation is diagnosed during the event, preventing the ascent of air parcels from within these valleys (not shown). Such downvalley flow has been previously observed on the southern

---

[3]The interpolation procedure is performed as follows: Along each trajectory, the point above maximum surface altitude between the intersection with the 50 km polygon and the arrival within the bounding box of the foehn valleys is identified, serving as definition for the crest. Subsequently, the upstream and downstream fragments of the trajectories are normalised to arrays of common length by linear interpolation. The temporal axis is therefore dimensionless, as the time required to cover upstream and downstream fragments can vary between trajectories.
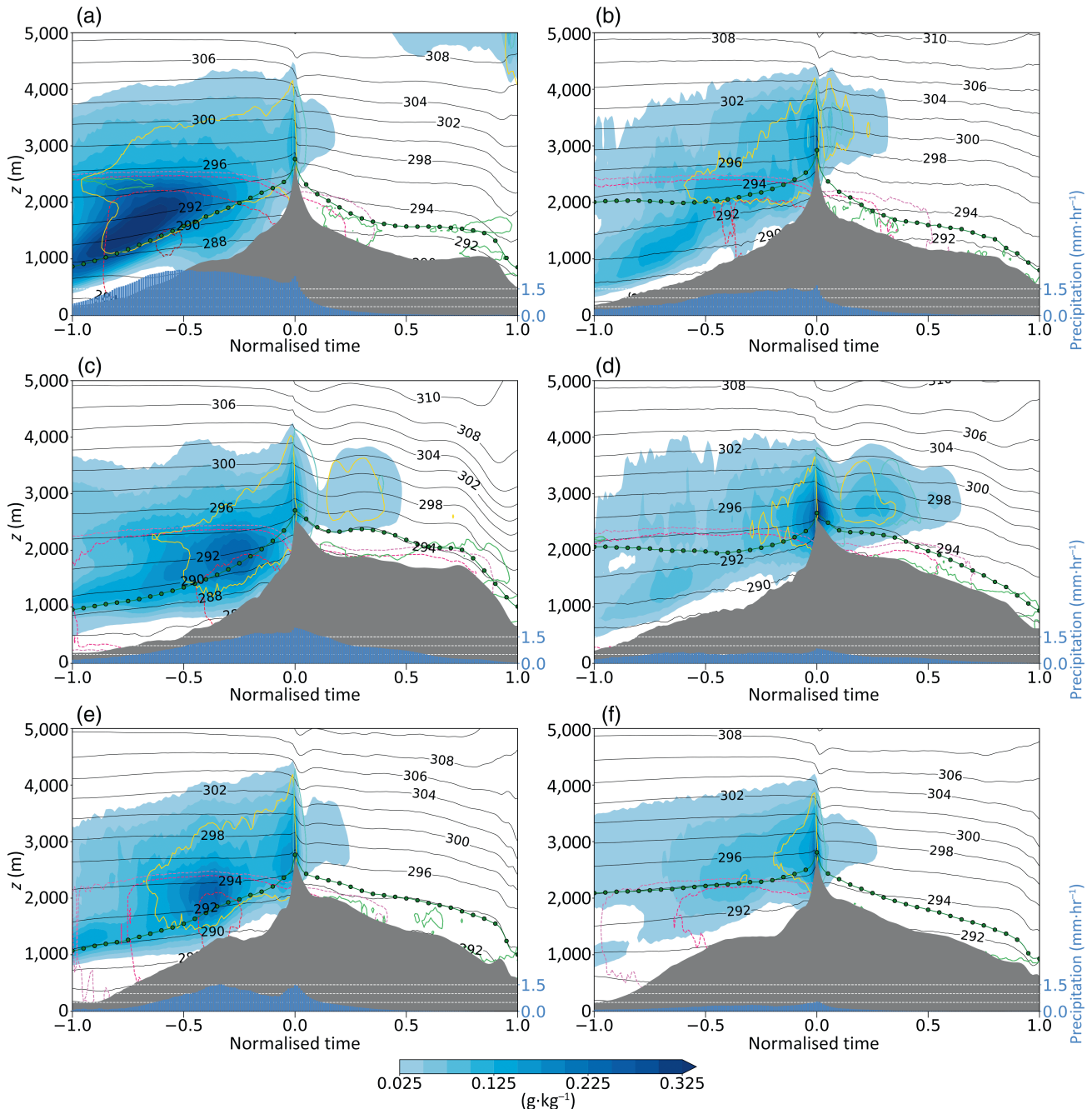
FIGURE 13 Normalised Lagrangian lidar plots for SHAS (left) and CAS trajectories (right) of (a, b) the Lower Valais, (c, d) the Reuss Valley, and (e, f) the Rhine Valley. Shown are the mean altitude of the trajectories (green line), cloud water and cloud ice in the column along the trajectory path (blue colour map), and the precipitating hydrometeor content (in pink to reddish contours for 0.005, 0.01, 0.05, 0.1 g·kg^{-1}). Isentropes are indicated as black contours, and the precipitation rate along the trajectory path is shown (blue bars at the bottom of the panels). Additionally, different contours for the diabatic temperature tendencies are shown: yellow indicates condensational heating (2 K·hr^{-1}), light-blue indicates evaporative cooling (−2 K·hr^{-1}) and light-green indicates turbulent cooling (−0.5 K·hr^{-1}) [Colour figure can be viewed at wileyonlinelibrary.com]

side of the Alps for orographic precipitation events (e.g., Bousquet and Smull, 2003). In agreement with the maxima of precipitating hydrometeors, intense precipitation rates are observed at the surface in the same regions, peaking at over 2 mm·hr^{-1} for the Lower Valais in the mean over all SHAS trajectories.

Shortly before reaching crest level, all trajectories experience a short time period of rapid ascent and, concurrently, a second maximum in cloud water, cloud ice, and surface precipitation. This pattern should, however, be considered with some caution, since it might partly be inherent to the crest definition of this study, which

prescribes an orographic obstacle before reaching the crest position and, therefore, favours peaks in cloud and precipitation shortly before arriving at crest level for all air parcels.

Considering Figure 13a,c,e, it is apparent that the airstream categorisation is not able to explain the full variance in between the valleys, since SHAS lidar scans of the Lower Valais and the Rhine Valley still exhibit considerable differences, whereby Rhine Valley trajectories are subject to less intense cloud and precipitation formation. However, the contrast between the different air-stream categories is of similar magnitude to the difference between the two valleys.

CAS trajectories pass through regions of considerably reduced cloud and precipitation formation as well as lower condensational heating (Figure 13b,d,e). Furthermore, they share a common original altitude of ~2 km. During their crest approach, the CAS air parcels are either transported along isentropes (Rhine Valley) or experience a slight diabatic descent (Lower Valais and Reuss Valley). Shortly before their arrival at the crest, they experience a brief period of enhanced diabatic ascent.

In the lee of the Alpine crest, all trajectories immediately experience a short time period of rapid cross-isentropic descent. The diabatic cooling in the first descent phase is mainly induced by the evaporation of remaining cloud and rain droplets in the air parcels (see light-blue contours in Figure 13). Furthermore, a striking feature is the vast downward advection of precipitating hydrometeors into the foehn valleys, especially for the Lower Valais and the Reuss Valley. This points out the potential for evaporative cooling during a significant time period of the descent, although the effect tends to be less important further away from the crest.[4] In most cases, trajectories experience a second, rapid descent prior to their arrival in the foehn valleys, where the air parcel transport is again cross-isentropic. This last phase potentially corresponds to the period where the air parcels are mixed with residual cold air pools within the valleys, thereby experiencing additional diabatic cooling due to turbulence (see light-green contours in Figure 13).

In summary, the different air-stream categories are clearly linked to a characteristic upstream cloud and precipitation pattern, although the categorisation cannot account for the full variability between the valleys. The cross-isentropic transport is related to distinct diabatic processes upwind of the Alps (condensational heating) and in the lee (evaporative cooling, turbulent

cooling). The upstream ascent of SHAS trajectories is found to happen preferably at the lower edge of the maxima in cloud hydrometeors and condensational heating. We interpret this finding invoking a buoyancy argumentation: Above this main ascent pathway, trajectories experience additional latent heating preventing a downstream descent into the valleys. Further below, trajectories are trapped within the blocked downvalley flow on the southern side of the Alps, preventing their ascent to crest level.

6 | CONCLUSIONS

In this study, a simulation with the kilometre-scale, limited-area model COSMO, including the calculation of online trajectories, was the basis for the application of a Lagrangian heat budget in order to study the foehn air warming and its associated airstreams in six major Alpine valleys. Thereby, the study focuses on a specific south foehn event lasting from November 20 to 24, 2016. The foehn event was induced by a distinct synoptic situation: Upstream upper-level Rossby wave breaking and cut-off formation led to a prolonged period of southwesterly large-scale flow conditions in the Alpine region and, therefore, to a foehn event of especially long duration. Intense orographic precipitation occurred during the event, particularly along the western slopes of the Alpine arc. The foehn intensity in the valleys varied in accordance with the evolution of the free tropospheric flow and the associated cross-Alpine pressure gradient, whereby differences between valleys can partly be attributed to different orientations of the valley axes.

The main goals of this study include a quantification of the Lagrangian warming and its decomposition into the contributing processes. Accordingly, the key findings of the first part can be formulated as follows.

- During the whole event, the majority of foehn air parcels experiences a net warming (92.6%), whereby the adiabatic warming exceeds the diabatic contribution for 57.2% of the air parcels. However, diabatic heating still constitutes the dominating warming mechanism for more than one-third of all air parcels (35.4%). Net cooling is, to a large extent, caused by adiabatic cooling and dominates in 6.8% of all air parcels.

- The net cross-Alpine vertical displacement of air parcels determines the sign and magnitude of the adiabatic temperature change. Strongly ascending trajectories experience more intense diabatic heating, but, at the same time, the adiabatic contribution decreases (or becomes negative) due to their low-level origin. Weakly

---

[4]Potentially, the evaporative cooling of descending air parcels can induce negative buoyancy and, therefore, contribute to a density-driven descent, a theory first proposed by Rossmann (1950). Future studies are necessary to elucidate the importance of this effect on descending air parcels.

ascending trajectories are subject to reduced diabatic heating (or diabatic cooling), though upstream adiabatic cooling diminishes simultaneously. Hence, the balance between these two mechanisms controls the temporal evolution of the net warming for the different valleys. This also points towards a complementary perspective on isentropic drawdown, whereby the net adiabatic effect is modulated by both the magnitude of the upstream adiabatic ascent and the downstream adiabatic descent.

- A distinct, three-phase evolution in the warming is observed during the event: Enhanced net warming mainly due to adiabatic descent during the first (November 19–20) and the last phases (November 24–25) is intercepted by reduced warming during the central phase (November 21–23). The western Alpine valleys show a clear decrease in the adiabatic warming and, concurrently, enhanced diabatic heating during this most intense, central period. The strong diabatic heating is partly able to overcompensate for the adiabatic cooling, thereby maintaining net warming for most air parcels.

- The upstream diabatic heating can almost completely be attributed to condensational heating in clouds, whereas downstream diabatic cooling is driven by both evaporative cooling of cloud and rain droplets as well as turbulent mixing. Radiative processes overall exhibit little impact on the diabatic heat budget.

The goals of the second part comprise the linkage of the thermodynamic history to distinct pathways of air parcels, as well as to the spatial and temporal characterisation of the airstreams identified. To this end, three types of thermodynamic airstreams are defined based on the net diabatic temperature change along trajectories, which were determined with the Lagrangian heat budget methodology. The three airstreams are referred to as SHAS (strong diabatic heating, $\Delta T_{\text{diab}} \geq 2.5$ K), WHAS (weak diabatic heating, 0 K $\leq \Delta T_{\text{diab}} < 2.5$ K), and CAS (diabatic cooling, $\Delta T_{\text{diab}} < 0$ K). The characteristics of these airstreams are as follows.

- The net diabatic temperature change is clearly linked to distinct airstreams: SHAS trajectories originate in the eastern Po Valley close to the surface. They are transported westward along the orographic obstacle in a low-level barrier jet before crossing the Alps ("Swiss foehn type"). On the other hand, CAS trajectories approach the Alps at ~2 km altitude without experiencing noteworthy ascent ("Austrian foehn type"). In between, a mixed variant exists incorporating characteristics from both these categories.

- These airstreams, in turn, exhibit a distinct temporal evolution in agreement with the heat budget analysis: SHAS trajectories are more important for the western Alpine valleys and during the central phase, whereas CAS trajectories become more relevant during the first and last phase of the event in all valleys.

- SHAS trajectories originate at ~1 km altitude and experience strong upstream cloud and precipitation formation. Their cross-isentropic ascent can be explained by condensational heating. In contrast, CAS trajectories are advected quasi-horizontally in drier environmental conditions. Downstream of the Alpine crest, a first phase of rapid descent is accompanied by the evaporation of the remaining cloud and rain droplets for most of the SHAS and CAS trajectories. Shortly before arrival in the foehn valleys, turbulent mixing close to the surface results in additional diabatic cooling for the trajectories of both air-stream categories.

Considering the different contributions of the heat budget along the airstreams, we gain an all-encompassing picture on the Lagrangian foehn air warming: SHAS trajectories originate from near-surface levels over the Po Valley. During their strong ascent, they experience intense latent heating. This heating compensates for the lack in net adiabatic warming compared with the air parcels of CAS, which are transported towards the Alps just below crest level, therefore experiencing less adiabatic cooling on the windward side. In summary, the Lagrangian warming of foehn air trajectories is always determined by the balance of diabatic heating they experience during the ascent, the magnitude of upstream ascent, and the elevation difference they are able to gain during the descent in the lee. In most cases, the downstream descent is expected to exceed the upstream ascent, so that the net adiabatic heating effect dominates the heat budget. In this case study, however, we illustrate that the "Swiss foehn type" can govern the overall warming for certain valleys and time periods if the atmospheric conditions are suitable. The findings thus also challenge the simplified distinction between the "Swiss foehn type" and the "Austrian foehn type", since the Lagrangian analysis reveals a continuum of mixed types, depending on the valley one focuses on or on the time period of an event.

When quantifying the foehn air warming, some caution is required regarding the frame of reference. As mentioned in Section 1, in a pure Eulerian framework, the warming depends on the precedent valley air mass (Glennf, 1961). As a first estimate for the cross-Alpine air mass change, surface potential temperature maps can be considered (Seibert, 1990). In a Lagrangian framework, the temperature change along an air parcel pathway is

quantified as the foehn air warming. However, even with the Lagrangian approach, it remains open which upstream point of reference has to be considered. Actually, Seibert (1990) pointed towards the fact that foehn air parcels originate from crest level, making their upstream history insignificant, since it does not matter for their lee-side warming whether they experienced prior ascent. However, this perspective neglects the physics of upstream processes and their potential effects on air parcel properties at crest level. For example, ascending air parcels in clouds can be more buoyant than air parcels subject to horizontal isentropic advection, which, in turn, affects their downstream behaviour. In a more holistic approach, Elvidge and Renfrew (2016) defined the foehn air warming as the temperature difference between the temperature of an air parcel after its lee-side descent and the temperature at the same level upwind of the orographic obstacle. Yet, depending upon the upstream stratification, this temperature difference can be smaller or larger than the actual Lagrangian temperature change along the air parcel pathway considered in this study.

Lastly, a few caveats of the study shall be discussed at this point, giving an outlook for possible future studies. Though the heat budget formulation (see Section 2.3) aims for a closed heat budget, outliers exist for trajectories experiencing unrealistically strong turbulence effects, especially if they are close to the surface (not shown). Possible reasons were mentioned in Section 2.3 and include numerical errors in the model (e.g., non-conservative advection) and errors arising from the trajectory calculation (e.g., the artificial lifting of terrain-intersecting trajectories). Furthermore, the reasons for the temporal evolution of the airstreams during the event remain open. We can only speculate about the possible roles of the shift in the large-scale flow direction (southwesterly to southeasterly), of a reduction in condensational heating due to a reduced moist inflow at low levels, and of a change in the Po Valley stratification. Future studies will focus on the role of the Po Valley stratification and the low-level easterly jet for the formation of these airstreams, and in particular for the SHAS airstream.

In summary, the results partly confirm earlier findings regarding the foehn air warming from Takane *et al.* (2015), Elvidge and Renfrew (2016), and Miltenberger *et al.* (2016), whereas the Lagrangian heat budget analysis is expanded to all diabatic tendencies and linked to distinct airstreams descending into major Alpine foehn valleys. Therefore, the study confirms the more balanced view of other recent studies on foehn air warming (Elvidge and Renfrew, 2016; Miltenberger *et al.*, 2016; Saigger and Gohm, 2022; Takane *et al.*, 2015). We thus want to point out that, usually, a combination of processes with varying relative contributions is responsible for the warming, instead of a pure thermodynamic or isentropic drawdown mechanism. The findings, however, are only based on one specific case study of an intense, long-lasting foehn period. An analysis of the foehn air warming and the presence of different airstreams for a multitude of different foehn flavours (moist foehn, dry foehn, shallow foehn, …) remains to be investigated in future studies.

AUTHOR CONTRIBUTIONS

Lukas Jansing: conceptualization; data curation; formal analysis; investigation; methodology; software; validation; visualization; writing – original draft. **Michael Sprenger:** conceptualization; funding acquisition; methodology; project administration; resources; supervision; validation; writing – review and editing.

ORCID

Lukas Jansing https://orcid.org/0000-0003-4644-5403

REFERENCES

Asano, Y. and Kusaka, H. (2021) Numerical simulation study of the effects of foehn winds on white head incidences in Yamagata Prefecture, Japan. *Meteorological Applications*, 28, e2042.

Bader, S., Begert, M., Coen, M.C., Frei, C., Fukutome, S., Gehrig, R., Barras, E.M., Philipona, R., Romanens, G. and Scherrer, S. (2017) *Klimareport 2016*. Zurich, Switzerland: MeteoSchweiz.

Baldauf, M., Seifert, A., Förstner, J., Majewski, D., Raschendorfer, M. and Reinhardt, T. (2011) Operational convective-scale numerical

weather prediction with the COSMO model: Description and sensitivities. *Monthly Weather Review*, 139, 3887–3905.

Ban, N., Schmidli, J. and Schär, C. (2014) Evaluation of the convection-resolving regional climate modeling approach in decade-long simulations. *Journal of Geophysical Research: Atmospheres*, 119, 7889–7907.

Beusch, L., Raveh-Rubin, S., Sprenger, M. and Papritz, L. (2018) Dynamics of a Puelche foehn event in the Andes. *Meteorologische Zeitschrift*, 27, 67–80.

Bougeault, P., Binder, P., Buzzi, A., Dirks, R., Houze, R., Kuettner, J., Smith, R.B., Steinacker, R. and Volkert, H. (2001) The MAP special observing period. *Bulletin of the American Meteorological Society*, 82, 433–462.

Bousquet, O. and Smull, B.F. (2003) Airflow and precipitation fields within deep Alpine valleys observed by airborne Doppler radar. *Journal of Applied Meteorology and Climatology*, 42, 1497–1513.

Drobinski, P., Steinacker, R., Richner, H., Baumann-Stanzer, K., Beffrey, G., Benech, B., Berger, H., Chimani, B., Dabas, A. and Dorninger, M. (2007) Föhn in the Rhine Valley during MAP: A review of its multiscale dynamics in complex valley geometry. *Quarterly Journal of the Royal Meteorological Society*, 133, 897–916.

Elvidge, A.D., Kuipers Munneke, P., King, J.C., Renfrew, I.A. and Gilbert, E. (2020) Atmospheric drivers of melt on Larsen C Ice Shelf: Surface energy budget regimes and the impact of foehn. *Journal of Geophysical Research: Atmospheres*, 125, e2020JD032463.

Elvidge, A.D. and Renfrew, I.A. (2016) The causes of foehn warming in the lee of mountains. *Bulletin of the American Meteorological Society*, 97, 455–466.

Elvidge, A.D., Renfrew, I.A., King, J.C., Orr, A. and Lachlan-Cope, T.A. (2014) Foehn warming distributions in nonlinear and linear flow regimes: A focus on the Antarctic Peninsula. *Quarterly Journal of the Royal Meteorological Society*, 142, 618–631.

Elvidge, A.D., Renfrew, I.A., King, J.C., Orr, A., Lachlan-Cope, T.A., Weeks, M. and Gray, S.L. (2015) Foehn jets over the Larsen C Ice Shelf, Antarctica. *Quarterly Journal of the Royal Meteorological Society*, 141, 698–713.

Gerstgrasser, D. (2017). Dokumentation Südföhn. MeteoSwiss internal report. 59 pp. (Available from the authors upon request.)

Glennf, C.L. (1961) The Chinook. *Weatherwise*, 14, 175–182.

Haid, M., Gohm, A., Umek, L., Ward, H., Muschinski, T., Lehner, L. and Rotach, M. (2020) Foehn–cold pool interactions in the Inn Valley during PIANO IOP2. *Quarterly Journal of the Royal Meteorological Society*, 146, 1232–1263.

Hann, J. (1866) Zur Frage über den Urpsrung des Föhn. *Zeitschrift der österreichischen Gesellschaft für Meteorologie*, 1, 257–263.

Hann, J. (1885) Einige Bemerkungen zur Entwickelungs-Geschichte der Ansichten über den Ursprung des Föhn. *Meteorologische Zeitschrift*, 20, 393–399.

Heise, E., Ritter, B. and Schrodin, R. (2006) *Operational implementation of the multilayer soil model* (COSMO Technical Report No. 9). Offenbach, Germany: Deutscher Wetterdienst.

Hermann, M., Papritz, L. and Wernli, H. (2020) A Lagrangian analysis of the dynamical and thermodynamic drivers of large-scale Greenland melt events during 1979–2017. *Weather and Climate Dynamics*, 1, 497–518.

Joos, H. and Wernli, H. (2012) Influence of microphysical processes on the potential vorticity development in a warm conveyor belt: A case-study with the limited-area model COSMO. *Quarterly Journal of the Royal Meteorological Society*, 138, 407–418.

Koyanagi, T. and Kusaka, H. (2020) A climatological study of the strongest local winds of Japan "Inami-kaze". *International Journal of Climatology*, 40, 1007–1021.

Kusaka, H., Nishi, A., Kakinuma, A., Doan, Q.-V., Onodera, T. and Endo, S. (2021) Japan's south foehn on the Toyama Plain: Dynamical or thermodynamical mechanisms? *International Journal of Climatology*, 41, 5350–5367.

Mattingly, K.S., Mote, T.L., Fettweis, X., Van As, D., Van Tricht, K., Lhermitte, S., Pettersen, C. and Fausto, R.S. (2020) Strong summer atmospheric rivers trigger Greenland Ice Sheet melt through spatially varying surface energy balance and cloud regimes. *Journal of Climate*, 33, 6809–6832.

Mellor, G.L. and Yamada, T. (1982) Development of a turbulence closure model for geophysical fluid problems. *Reviews of Geophysics*, 20, 851–875.

Miltenberger, A.K., Pfahl, S. and Wernli, H. (2013) An online trajectory module (version 1.0) for the nonhydrostatic numerical weather prediction model COSMO. *Geoscientific Model Development*, 6, 1989–2004.

Miltenberger, A.K., Reynolds, S. and Sprenger, M. (2016) Revisiting the latent heating contribution to foehn warming: Lagrangian analysis of two foehn events over the Swiss Alps. *Quarterly Journal of the Royal Meteorological Society*, 142, 2194–2204.

Montecinos, A., Muñoz, R.C., Oviedo, S., Martínez, A. and Villagrán, V. (2017) Climatological characterization of Puelche winds down the western slope of the extratropical Andes Mountains using the NCEP Climate Forecast System Reanalysis. *Journal of Applied Meteorology and Climatology*, 56, 677–696.

Nannoni, A., Vigna, B., Fiorucci, A., Antonellini, M. and De Waele, J. (2020) Effects of an extreme flood event on an alpine karst system. *Journal of Hydrology*, 590, 125493.

Papritz, L. and Pfahl, S. (2016) Importance of latent heating in mesocyclones for the decay of cold air outbreaks: A numerical process study from the Pacific sector of the Southern Ocean. *Monthly Weather Review*, 144, 315–336.

Raschendorfer, M. (2001). The new turbulence parameterization of LM. In G. Doms & U. Schättler (Eds.), *COSMO Newsletter No. 1*, pp. 89–97. Offenbach, Germany: Deutscher Wetterdienst.

Reinhardt, T. and Seifert, A. (2006). A three-category ice scheme for LMK. In U. Schättler, A. Montani, & M. Milelli (Eds.), *COSMO Newsletter No. 6*, pp. 115–120. Offenbach, Germany: Deutscher Wetterdienst.

Richner, H., Baumann-Stanzer, K., Benech, B., Berger, H., Chimani, B., Dorninger, M., Drobinski, P., Furger, M., Gubser, S. and Gutermann, T. (2006) Unstationary aspects of foehn in a large valley part I: operational setup, scientific objectives and analysis of the cases during the special observing period of the MAP subprogramme FORM. *Meteorology and Atmospheric Physics*, 92, 255–284.

Richner, H. and Hächler, P. (2013). Understanding and forecasting Alpine foehn. In F.K. Chow, S.F. De Wekker, & B.J. Snyder (Eds.), *Mountain weather research and forecasting: Recent progress and current challenges*, pp. 219–260. Dordrecht, Netherlands: Springer.

Ritter, B. and Geleyn, J.-F. (1992) A comprehensive radiation scheme for numerical weather prediction models with potential applications in climate simulations. *Monthly Weather Review*, 120, 303–325.

Rossmann, F. (1950) Über das Absteigen des Föhns in die Täler. *Berichte des deutschen Wetterdienstes der US-Zone*, 12, 94–98.

Rotunno, R. and Houze, R.A. (2007) Lessons on orographic precipitation from the Mesoscale Alpine Programme. *Quarterly Journal of the Royal Meteorological Society*, 133, 811–830.

Saigger, M. (2021). *Is it north or west foehn? A Lagrangian analysis of PIANO IOP 1* (Master's thesis). University of Innsbruck, Innsbruck, Austria.

Saigger, M. and Gohm, A. (2022) Is it north or west foehn? A Lagrangian analysis of PIANO IOP 1. *Weather and Climate Dynamics*, 3, 279–303.

Sandner, V. (2020). *Verification of COSMO-1 forecasts of foehn breakthrough and interruption in the region of Innsbruck* (Master's thesis). University of Innsbruck, Innsbruck, Austria.

Schmidli, J., Böing, S. and Fuhrer, O. (2018) Accuracy of simulated diurnal valley winds in the Swiss Alps: Influence of grid resolution, topography filtering, and land surface datasets. *Atmosphere*, 9, 196.

Schneidereit, M. and Schär, C. (2000) Idealised numerical experiments of Alpine flow regimes and southside precipitation events. *Meteorology and Atmospheric Physics*, 72, 233–250.

Seibert, P. (1985) *Fallstudien und statistische Untersuchungen zum Südföhn im Raum Tirol* (PhD thesis). University of Innsbruck, Innsbruck, Austria.

Seibert, P. (1990) South foehn studies since the ALPEX experiment. *Meteorology and Atmospheric Physics*, 43, 91–103.

Seibert, P. (2005) Hann's thermodynamic foehn theory and its presentation in meteorological textbooks in the course of time, From Beaufort to Bjerknes and beyond, Algorismus, 52, 169–180.

Seibert, P., Feldmann, H., Neininger, B., Bäumle, M. and Trickl, T. (2000) South foehn and ozone in the eastern Alps—case study and climatological aspects. *Atmospheric Environment*, 34, 1379–1394.

Sharples, J.J., Mills, G.A., McRae, R.H. and Weber, R.O. (2010) Foehn-like winds and elevated fire danger conditions in southeastern Australia. *Journal of Applied Meteorology and Climatology*, 49, 1067–1095.

Smith, R.B., Jiang, Q., Fearon, M.G., Tabary, P., Dorninger, M., Doyle, J.D. and Benoit, R. (2003) Orographic precipitation and air mass transformation: An Alpine example. *Quarterly Journal of the Royal Meteorological Society*, 129, 433–454.

Sprenger, M., Dürr, B. and Richner, H. (2016). Foehn studies in Switzerland. In S. Willemse & M. Furger (Eds.), *From weather observations to atmospheric and climate sciences in Switzerland: Celebrating 100 years of the Swiss Society for Meteorology*, pp. 215–248. Zurich, Switzerland: vdf Hochschulverlag AG.

Sprenger, M., Schemm, S., Oechslin, R. and Jenkner, J. (2017) Nowcasting foehn wind events using the AdaBoost machine learning algorithm. *Weather and Forecasting*, 32, 1079–1099.

Steinacker, R. (2006) Alpiner Föhn—Eine neue Strophe zu einem alten Lied. *Promet*, 32, 3–10.

Steppeler, J., Doms, G., Schättler, U., Bitzer, H., Gassmann, A., Damrath, U. and Gregoric, G. (2003) Meso-gamma scale forecasts using the nonhydrostatic model LM. *Meteorology and Atmospheric Physics*, 82, 75–96.

Takane, Y. and Kusaka, H. (2011) Formation mechanisms of the extreme high surface air temperature of 40.9°C observed in the Tokyo metropolitan area: Considerations of dynamic foehn and foehnlike wind. *Journal of Applied Meteorology and Climatology*, 50, 1827–1841.

Takane, Y., Kusaka, H. and Kondo, H. (2015) Investigation of a recent extreme high-temperature event in the Tokyo metropolitan area using numerical simulations: the potential role of a 'hybrid' foehn wind. *Quarterly Journal of the Royal Meteorological Society*, 141, 1857–1869.

Umek, L., Gohm, A., Haid, M., Ward, H. and Rotach, M. (2021) Large-eddy simulation of foehn–cold pool interactions in the Inn Valley during PIANO IOP 2. *Quarterly Journal of the Royal Meteorological Society*, 147, 944–982.

Walker, A. and Ruffner, H. (1998) Föhnforschung und Traubenreife. *Schweizer Zeitschrift für Obst- und Weinbau*, 9/98, 245–247.

Wilhelm, M. (2012). *COSMO-2 model performance in forecasting foehn: A systematic process-oriented verification* (Master's thesis). MeteoSchweiz, Bundesamt für Meteorologie und Klimatologie, Zurich, Switzerland.

Würsch, M. and Sprenger, M. (2015) Swiss and Austrian foehn revisited: A Lagrangian-based analysis. *Meteorologische Zeitschrift*, 24, 225–242.

SUPPORTING INFORMATION

Additional supporting information may be found online in the Supporting Information section at the end of this article.